Performance Evaluation of DOA Algorithms for Non-uniform Linear Arrays in a Weather-Impacted Environment

B. P. Nxumalo[1], and T. Walingo[2]

[1, 2] Discipline of Electrical, Electronic and Computer Engineering, University of KwaZulu-Natal, Durban 4041, Republic of South Africa.

Corresponding author: Bongani Prudence Nxumalo (nxumalobonganip@gmail.com)

Key Points:

- The performance of Minimum Variance Distortionless Response (MVDR), Multiple Signal Classification (MUSIC) and the proposed Advanced-MUSIC (A-MUSIC) non-uniform linear array (NLA) algorithms on a weather impacted wireless channel is investigated.
- The co-prime and array interpolation NLA configurations are investigated on a markovian rainfall channel model capturing widespread, shower and thunderstorm rain events.
- The results indicate that the algorithms experience severe performance degradation in a weather affected environment. However, the developed NLA algorithm achieves better Direction of Arrival (DOA) estimation than the conventional NLA.

Abstract

Spectrum scarcity has necessitated the migration of radio frequencies from the lower to the higher frequencies. This has resulted in radio propagation challenges due to the adverse environmental elements otherwise unexperienced at lower frequencies. A re-design and re-evaluation of the performance of traditional lower frequency technologies and algorithms for implementation at higher frequencies especially for non-uniform linear antenna arrays are therefore necessary. Specifically, the performance of Direction of Arrival (DOA) algorithms for non-linear antenna arrays on weather impacted environments needs to be quantified and new algorithms developed to counteract the migration challenges. This work investigates the performance of Minimum Variance Distortionless Response (MVDR), Multiple Signal Classification (MUSIC) and the proposed Advanced-MUSIC (A-MUSIC) non-uniform linear array (NLA) algorithms on a weather-impacted wireless channel. The results indicate that the developed NLA achieves better DOA estimation than the conventional NLA albeit at a reduced performance for both, in a weather-impacted scenario.

1 Introduction

Direction of Arrival (DOA) estimation is critical in antenna design for emphasizing the desired signal and minimizing interference. Smart antenna systems utilize DOA algorithms to estimate the beamforming vectors, to track and identify the antenna beam, making DOA estimation critical in smart antenna design and beamforming (Krim et al., 1996). The accurate estimation of the DOA of the transmitted signals at the adaptive array antenna results in improved performance in the recovery of the transmitted signal and suppression of other interfering signals. The motivation for adopting Non-Uniform Linear Arrays (NLA) as opposed to the Uniform Linear Arrays (ULA) include the following (El kassis, et al., 2010; Saric et al., 2010): Firstly, the failure of any antenna sensor element(s) renders ULA to become NLA in harsh applications field and this could lead to data loss. Secondly, physical and geographical conditions may prohibit the construction of uniformly spaced sensors leading to NLA. Thirdly, the need to reduce the number of sensors to decrease the production cost and minimize the impact on performance, and finally the need to increase the aperture of an antenna using the same number of sensors in order to obtain better performance, among others. NLA allow better resolution for the same number of array elements compared to the ULA. Generally, NLA have larger antenna aperture, smaller main lobe width resulting in better performance in angle resolution, estimation precision, and other aspects. Therefore, the performance of NLA is of paramount importance especially with the migration to higher frequencies that are more susceptible to the adverse weather environmental factors.

Estimation accuracy of a given array depends upon characteristics of the array geometry and the employed estimation algorithm; therefore, accurate DOS algorithms are required. DOA estimation for NLA is more critical. Their uneven number of source and receiver antennas leads to different degrees of freedom and irregular geometry. This results in different antenna sensor separation and aperture sizes. Furthermore, the migration to higher frequencies makes it worse due to the adverse effect of weather elements at these frequencies. New geometries requiring different degrees of freedom for NLA have been proposed (Vaidyanathan et al., 2011; Tan et al., 2014). They involve the studying of the covariance matrix of the received signals among different sensors. Sparse arrays can be considered as a ULA where some sensors are omitted or irregular linear arrays where the inter-sensor separations are chosen in an arbitrary way (Choi et al., 2010). The irregular spacing results in difficulties in covariance between the various elements because of the mutual coupling. These factors make DOA estimation for NLA challenging. NLAs give similar performance to ULA with a smaller number of physical elements. Co-prime array (Vaidyanathan et al., 2011; Tan et al., 2014) and array interpolation (Bronez et al., 1988; Friedlander et al., 1993) have become the most popular algorithms for evaluating NLA. A co-prime array comprises of two spatially under-sampled ULAs with co-prime spatial sampling rates (Vaidyanathan et al., 2011; Pal et al., 2011). Array interpolation maps the covariance matrix of a real array to a virtual array and enables the reduction of DOA estimation problems in NLA to much simpler virtual ULA problems. Both these algorithms are investigated in this work for NLA in a weather-impacted environment.

The most popular DOA algorithms used include the Minimum Variance Distortionless Response (MVDR) algorithm that enforces a unit response at the direction of the desired signal and places nulls in the directions of the interferences (Yu et al., 2015). The Multiple Signal Classification (MUSIC) algorithm and its variants is applied directly to the NLA geometry resulting in high computational complexity due to the multiple search for the maximum (Abramovich et al., 1999). This work proposes the Advanced-MUSIC (A-MUSIC) DOA algorithm that employs forward-backward averaging preprocessing technique on the cross correlation of array output to improve the performance of the DOA techniques for NLAs. The application of these techniques in a weather impacted radio propagation scenario for NLA is challenging and is the focus of this work.

The increasing demand on mobile broadband services has led to the scarcity of radio spectrum due to spectrum exhaustion (Zhang et al., 2015). This has led to migration to higher frequency millimetre-wave (mmW) bands, which range from 30 GHz to 300 GHz, for mmW communication with additional large bandwidths. Apart from the merits of increased bandwidth and high frequency reuse packing due to shorter wavelengths, mmW communication possesses its own challenges including large path loss suffered by mmW signals and the effect of the weather effectors to signals in this band. Rainfall is a common weather phenomenon that affects signal transmission at this band. In link budget design at lower frequencies, rainfall is considered as a fixed propagation attenuation taken into account in the planning (Pi et al., 2011). The signal suffers from absorption from the rain causing signal attenuation. Apart from attenuation, the signals undergo scattering when transmitted through rain leading to both amplitude attenuation and phase fluctuation (Ishimaru et al., 2004). Rain attenuation and scattering are a function of the rain rate, polarization, physical size of drops and operating frequency (Agber et al., 2013; Calla et al., 1990). Rainfall attenuation, frequency attenuation and phase distortion affect the received signal. It is therefore mandatory for DOA algorithms to consider weather effects for the systems. This has rarely been done in literature and therefore, addressed in this work.

The performance of the DOA algorithms for NLA in weather affected channels needs to be evaluated. Moreover, better DOA algorithms design is required to mitigate against the weather effects. This work investigates and compares the performance of the NLA DOA algorithms on a rainfall-impacted network and develops a hybrid algorithm to combat the weather effects. We employ realistic markovian rainfall channel model to accurately capture the rainfall variations in the following cases: widespread, shower and thunderstorm rain events.

The structure of this paper is organized as follows. Section 2 presents the NLA system model. Section 3 presents the evaluation of NLA as co-prime array or with array interpolation. In section 4, the weather impacted propagation channel is modelled. The proposed method for efficiently estimating the DOA and other conventional and subspace DOA estimation algorithms are presented in section 5. In section 6, the performance measures and overall performance evaluation algorithm are presented. The simulation results and discussion are presented in section 7 and the main conclusions drawn from them summarized in section 8.

Notation: The bold upper- and lower-case letters represent the matrices and column vectors, respectively. I is an identity matrix. The following superscripts $(\cdot)^*$,$(\cdot)^H$,$(\cdot)^{-1}$ and $(\cdot)^T$ represent optimality, Hermitian, inverse and transpose operators, respectively and $E\{\cdot\}$ is the mathematical expectation. d is the spacing difference between array elements, c is the speed of light and λ is the wavelength.

2 System model

The system model consists of a source transmitting a signal $s(t)$ that traverses through a weather-impacted environment to impinge on the antenna elements at an angle θ. Assuming there are K uncorrelated narrowband plane-wave signals. The signals $x(t)$ induced on the antenna arrays are multiplied by adjustable complex weights w and then summed to form the system output $y(t)$.

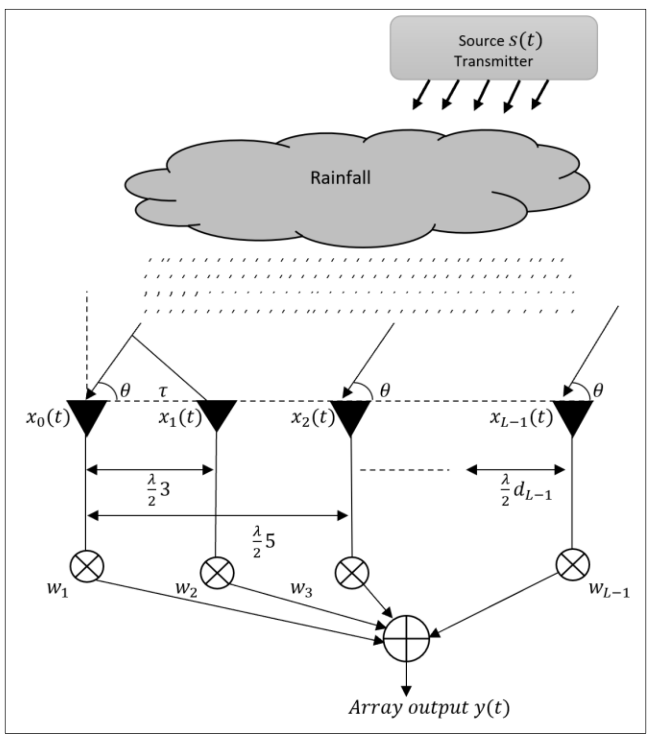

Figure 1: Non-uniform linear array

A sparse NLA is considered with L existing elements. The sensors are separated with a distance d_i, a multiple of a half wavelength from each other. As shown in Fig.1, the array has configuration, $D = [d_1, d_2, \ldots, d_{L-1}]$ such that $d = \lambda/2 * [0, d_2, \ldots, d_{L-1}]$. The system is assumed to be confined to an azimuth-only system with isotropic sensors.

The received signal on the l^{th} element at the t^{th} snapshot is expressed as

$$x_l(t) = \sum_{i=1}^{K} \alpha_i s_i(t)\, a_i(\theta_i + \Delta\theta_i) + v_i(t) \quad \text{for} \quad i = 1,2, \ldots K, \tag{1}$$

where α_i is the rainfall attenuation, θ_i the angle of arrival, $\Delta\theta_i$ the rainfall angle deviation, $s_i(t)$ is signal associated with the i^{th} wave front and $v_i(t)$ is the additive white Gaussian noise at the l^{th} element. The total received signal vector X is expressed as:

$$X = A(\hat{\theta})\tilde{S}(t) + V(t), \tag{2}$$

where

$$X = [x_1(t), x_2(t), \ldots, x_K(t)]^T,$$

$$A(\hat{\theta}) = \left[a_1(\hat{\theta}_1), a_2(\hat{\theta}_2), \ldots, a_K(\hat{\theta}_K)\right]^T,$$

$$\tilde{S}(t) = [\tilde{s}_1(t), \tilde{s}_2(t), \ldots, \tilde{s}_K(t)]^T,$$

$$V(t) = [v_1(t), v_2(t), \ldots, v_K(t)]^T, \tag{3}$$

where $\tilde{s}_i(t) = \alpha_i s_i(t)$ and $\hat{\theta}_i = \theta_i + \Delta\theta_i$. The modelling and investigation of the rainfall attenuation α_i and angle deviation $\Delta\theta_i$ due to the weather impacted rainfall channel for NLA is the key focus on this work.

3 NLA methods

3.1 Co-prime Array Scheme

The NLA with L elements is divided into a co-prime array comprising of two spatially under sampled ULAs with co-prime spatial sampling rates (Vaidyanathan et al., 2011; Pal et al., 2011). This work utilizes the extended co-prime array configuration proposed in (Pal et al., 2011). In this configuration, the array is a union of two ULAs, one with N sensors and spacing Md and the other with sensors $2M - 1$ and spacing Nd as shown in the Fig. 2, where $d = \lambda/2$ to avoid spatial aliasing. The total number of physical elements is L= $2M + N - 1$.

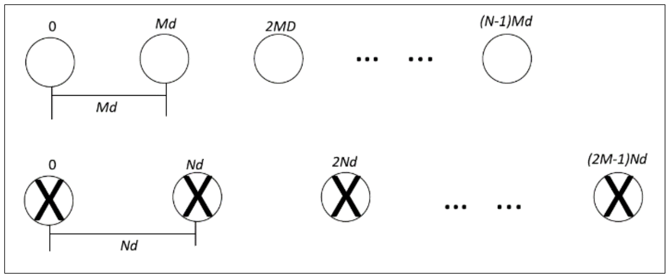

Figure 2: Co-prime array

Denote $d_i = \lambda/2 \, * [0, d_2, \dots, d_{L-1}]$ as the positions of the array sensors where $i = 1, \dots, 2M + N - 1$, the first sensor is assumed as the reference, i.e., $d_1 = 0$. From equation (1) the data vector received at the co-prime array is expressed as

$$x_l(t) = \sum_{i=1}^{K} \alpha_i s_i(t)\, a_i(\theta_i + \Delta\theta_i) + v_i(t), \tag{4}$$

where

$$a_i(\hat{\theta}_i) = [1, e^{\frac{2\pi d_2}{\lambda}\sin(\hat{\theta}_i)}, \dots, e^{\frac{2\pi d_2 L}{\lambda}\sin(\hat{\theta}_i)}]^T, \tag{5}$$

is the steering vector of the array corresponding to $\hat{\theta}_i$. The elements of the noise vector $v(t)$ are assumed to be independent and identically distributed $(i.i.d)$ random variables with a complex Gaussian distribution. The received signal vectors are similarly defined as in equation (2) and (3). The covariance matrix of data vector $x_l(t)$ is obtained as (Zhang et al., 2014)

$$\begin{aligned}\sigma(x,x) &= E[x_l(t)\, x_l^H(t)] = A\sigma(s,s)A^H + \vartheta^2 I \\ &= \sum_{i=1}^{K} \rho_i^2 a(\hat{\theta}_i) a^H(\hat{\theta}_i) + \vartheta^2 I,\end{aligned} \tag{6}$$

where $\sigma(s,s) = E[s_l(t) s_l^H(t)] = diag([\rho_1^2, \dots, \rho_I^2])$ is the source covariance matrix, $diag(\cdot)$ denotes a diagonal matrix that uses the elements of a vector as its diagonal elements, ρ_i^2 denotes the input signal power of the i^{th} signal, ϑ^2denotes the noise variance and I is the identity matrix. In practice, the exact covariance matrix $\sigma(x,x)$ is approximated by its sample estimate $\hat{\sigma}(x,x)$ using the available Z snapshots, given by

$$\hat{\sigma}(x,x) = \frac{1}{Z}\sum_{j=1}^{Z} x_l(t)\, x_l^H(t). \tag{7}$$

The sample covariance matrix $\hat{\sigma}(x,x)$ approaches the theoretical version $\sigma(x,x)$ as the number of snapshots tends to infinity. The covariance matrix is utilised by the applied coprime DOA algorithms of section 5.

3.2 Modified Array Interpolation Scheme

The implemented interpolation considers an interpolation sector $[\theta_b, \theta_f]$ with the source DOA's assumed to be inside the sector $\hat{\theta} \in [\theta_b, \theta_f]$. The interpolation sector is uniformly divided into

$\Delta\theta$ intervals such that $\hat{\theta}_i = i\Delta\theta, i = 0\ to \lfloor (\theta_f - \theta_b)/\Delta\theta \rfloor$. With $A(\hat{\theta})$ and $\bar{A}(\hat{\theta})$ the manifold matrices of ULA and NLA respectively, the mapping matrix of the conventional interpolation array B is given by (Tuncer et al., 2007; Li et al., 2014)

$$B = (A(\hat{\theta})A(\hat{\theta})^H)^{-1}A(\hat{\theta})\bar{A}(\hat{\theta})^H, \tag{8}$$

Then an interpolation matrix B is designed to satisfy the least squares problem i.e.

$$\min_B \left\| B^H A(\hat{\theta}) - \bar{A}(\hat{\theta}) \right\|_F^2,$$
(9)

where $\|\cdot\|_F$ denotes the Frobenius norm of a matrix. The finite interpolation points results in interpolation mapping errors making the estimations not statistically optimal (Belloni et al., 2007). To alleviate this, the new transformation matrix G is reconstructed by projecting the transformational matrix with the sample array covariance matrix

$$G = (\bar{B}^H\bar{B})^{-1/2}\bar{B}^H, \tag{10}$$

where $\bar{B} = \hat{\sigma}(x,x)B$. The real antenna array steering vector $a(\hat{\theta})$ and the virtual array steering vector $\bar{a}(\hat{\theta})$ have the following relationship, $Ga(\hat{\theta}) = (\bar{B}^H\bar{B})^{-\frac{1}{2}}\bar{a}(\hat{\theta}) = \hat{\bar{a}}(\hat{\theta})$. As a result of noise pre-whitening for cases where background noise becomes non-Gaussian after virtual transformation. The covariance matrix of the virtual antenna can be computed by using the transformation matrix G as (Li et al., 2014) as

$$\hat{\bar{\sigma}}(x,x) = G\sigma(x,x)G^H = \hat{\bar{A}}\sigma(s,s)\hat{\bar{A}}^H + \vartheta^2 I, \tag{11}$$

with $\hat{\bar{\sigma}}(x,x)$ the covariance matrix and array manifold $\hat{\bar{A}}$ are the pre-whitened values of the virtual antenna array and $\sigma(s,s) = E[s_l(t)s_l^H(t)]$. The covariance matrix is utilised by the applied DOA algorithms of section 5.

4 Weather channel parameter modelling

4.1 Rainfall modelling

The signal attenuation magnitude largely depends on the rain intensity. Based on its intensity, rain event may be classified into drizzle (D), widespread (W), shower (S) and thunderstorm (T). Table 1 presents the rain intensities of the four classes of rain. The rainfall is modelled by four or fewer states of a Markov Chain, R, given by

$$\mathrm{R} = \{\mathrm{D}, \mathrm{W}, \mathrm{S}, \mathrm{T}\}. \tag{12}$$

Table 1. Rain Rate Categories

Description	**Rain Rate (r)**	**Steady state**

	mm\hr	**prob.** π_n
Drizzle	1-5	π_D
Widespread	5-10	π_W
Shower	10-40	π_S
Thunderstorm	>40	π_T

Practical rainfall, widespread, shower and thunderstorm events consist of a mix of the different rain events (Alonge et al., 2015). This work utilizes Markov models developed from actual rain data to model practical rain events, with the state transition diagram and state transition probabilities as given below:

i) Widespread rainfall: Consists of drizzle and widespread events. The markovian transition among states in this event is shown in Fig. 3, with the transition probabilities, $P_{i,j}^{W}$, form state i to j, with $i, j \in R$ given by equation (13)

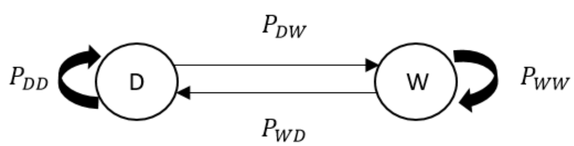

Figure 3: Widespread rainfall.

$$P_{i,j}^{W} = \begin{bmatrix} P_{DD} & P_{DW} \\ P_{WD} & P_{WW} \end{bmatrix}, \tag{13}$$

where P_{DW} is the transition from drizzle to widespread, P_{WD} is the transition from widespread to drizzle, P_{DD} is the no transition from drizzle and P_{WW} is the no transition from widespread.

ii) Shower rainfall consists of drizzle, widespread and shower events. The markovian transition among states in this event is shown in Fig. 4, with the transition probabilities, $P_{i,j}^{S}$, form state i to j, with $i, j \in R$ given by equation (14)

$$P_{i,j}^{S} = \begin{bmatrix} P_{DD} & P_{DW} & P_{DS} \\ P_{WD} & P_{WW} & P_{WS} \\ P_{SD} & P_{SW} & P_{SS} \end{bmatrix}, \tag{14}$$

where P_{DS} is the transition from drizzle to shower, P_{WS} is the transition from widespread to shower, P_{SD} is the transition from shower to drizzle, P_{SW} is the transition from shower to widespread and P_{SS} is the no transition from shower.

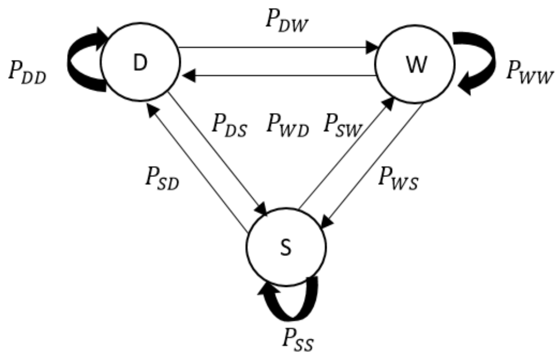

Figure 4: Shower rainfall

iii) Thunderstorm rainfall consists of drizzle, widespread, shower and thunderstorm events. The markovian transition among states in this event is shown in Fig. 5, with the transition probabilities, $P_{i,j}^{T}$, form state i to j, with $i, j \in R$ given by equation (15)

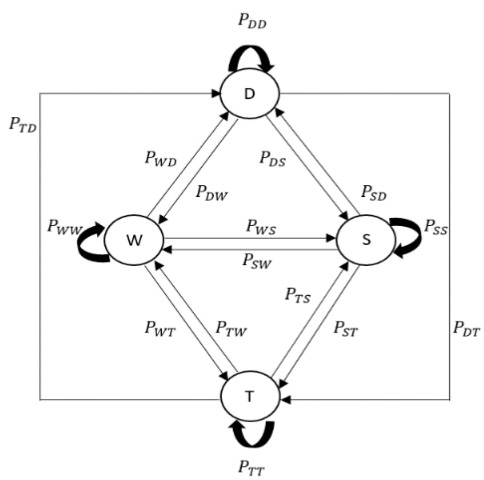

Figure 5: Thunderstorm rainfall

$$P_{i,j}^{T} = \begin{bmatrix} P_{DD} & P_{DW} & P_{DS} & P_{DT} \\ P_{WD} & P_{WW} & P_{WS} & P_{WT} \\ P_{SD} & P_{SW} & P_{SS} & P_{ST} \\ P_{TD} & P_{TW} & P_{TS} & P_{TT} \end{bmatrix}, \quad (15)$$

where P_{DT} is the transition from drizzle to thunderstorm, P_{WT} is the transition from widespread to thunderstorm, P_{ST} is the transition from shower to thunderstorm, P_{TD} is the transition from thunderstorm to drizzle, P_{TW} is the transition from thunderstorm to widespread, P_{TS} is the transition from thunderstorm to shower and P_{TT} is the no transition from thunderstorm.

The transition probabilities used are practically obtained as in (Alonge et al., 2015). The steady state probability of an event $n, \pi_n = \{\pi_D, \pi_W, \pi_S, \pi_T\}$, is solved by the standard Markov chain solution methods. The expected rate for a rainfall occurrence is derived from the probabilities as

$$E[r] = \sum_n r_n \pi_n, \tag{16}$$

where r_n is the mean rain event and π_n is the steady state probability of the n^{th} state of the Markov model. The actual rain rate r is computed from a lognormal distribution with the given mean (Kedem et al., 1987; Cho et al., 2004).

4.2 Attenuation model

We consider a radio propagation environment where the signal is affected by attenuation due to the weather-impacted factors. The total attenuation A_T is given by

$$A_T = \alpha_r + L_{fs}, \tag{17}$$

where α_r is the rain attenuation. The ITU rainfall model (I.T.U et al., 2005) is used for attenuation as

$$\alpha_r = cr^a, \tag{18}$$

where r is the expected rain rate. The parameter c and exponent a depend on the frequency, f(GHz), the polarization state, and the elevation angle of the signal path. Free space loss attenuation, L_{fs} is given by

$$L_{fs} = 20 * \log_{10}\left(\frac{4\pi d}{\lambda}\right), \tag{19}$$

where λ is the signal wavelength in metres and d is the distance from the transmitter.

4.3 Angle deviation model

The weather factors result in the delay and scattering of the transmitted signal leading to a phase angle change, the angle deviation. The angle deviation, $\Delta\theta_i$, is modelled as a normal distributed random variable with a mean μ_θ bounded as follows

$$\Delta\theta_{min} \leq \Delta\theta_i \leq \Delta\theta_{max}, \tag{20}$$

where $\Delta\theta_{min}$ and $\Delta\theta_{max}$ are the minimum and maximum angle deviations respectively. The mean μ_θ is derived from the normalized rain rate

$$\mu_\theta = r/r_{max}, \tag{21}$$

and r_{max} is the maximum rain rate. The assumption is reasonable as the heavier the rain, the more the scattering. The standard deviation is kept constant.

5 DOA Estimation Algorithms

5.1 MVDR Algorithm

5.1.1 MVDR Co-prime NLA

The MVDR algorithm minimizes the output power and constrains the gain in the direction of desired signal to unity as follows (Yu et al., 2015),

$$minE\{|y_i(t)|^2\} = min\, w^H \hat{\sigma}(x,x)w\ , \tag{22}$$

subject to $w.a(\hat{\theta}) = 1$, where $y_i(t)$ is the output of the array system and is given by

$$y_i(t) = w^H \hat{\sigma}(x,x)w. \tag{23}$$

The weight vector w is given by

$$w = \frac{(\hat{\sigma}(x,x))^{-1}a(\hat{\theta})}{a^H(\hat{\theta})(\hat{\sigma}(x,x))^{-1}a(\hat{\theta})}\ , \tag{24}$$

where $\hat{\sigma}(x,x)$is covariance matrix of the received signal for the L number of elements given by equation (7). H is the Hermitian matrix and $a(\hat{\theta})$ is the steering vector. The MVDR spatial spectrum is defined by

$$P_{MVDR\_Co-Prime} = \frac{1}{a^H(\hat{\theta})(\hat{\sigma}(x,x))^{-1}a(\hat{\theta})}. \tag{25}$$

The computational steps of MVDR algorithm using co-prime array are summarized in Algorithm 1.

Algorithm 1: MVDR Algorithm using Co-prime array

1. **Input:** $x = \{x_i(t)\} = f(\alpha_i, \hat{\theta}_i)$, M, N, L, K, d, λ, Z and $\mu \leftarrow$ Step size
2. Compute covariance matrix $\hat{\sigma}(x,x)$equation (7)
3. Compute the weight vector w, equation (24)
4. Compute the output array system $y_i(t)$, equation (23)
5. while $w.a(\hat{\theta}) \neq 1$
  do Minimize the output power, equation (22),
  Subject to $w.a(\hat{\theta}) = 1$,
6. Compute MVDR spectrum for co-prime array, equation (25)

5.1.2 MVDR Interpolation NLA

The spectrum of MVDR by array interpolation is given by (Friedlander et al., 1992)

$$P_{MVDR\_AI} = \frac{1}{a^H(\hat{\theta})(\hat{\hat{\sigma}}(x,x))^{-1}a(\hat{\theta})}, \tag{26}$$

where $a(\hat{\theta})$ is the steering vector and $\hat{\hat{\sigma}}(x,x)$ is the covariance matrix of the virtual antenna derived in equation (11). The computational steps of MVDR array interpolation algorithm are summarized in Algorithm 2.

Algorithm 2: MVDR Algorithm using array interpolation

1. **Input:** $x = \{x_i(t)\} = f(\alpha_i, \hat{\theta}_i)$, M, N, L, K, d, λ, Z and $\mu \leftarrow$ Step size
2. Determine the ULA array manifold $A(\hat{\theta})$
3. Compute the real array covariance matrix $\hat{\sigma}(x,x)$ equation (7)
4. Compute the virtual array manifold $\bar{A}(\hat{\theta})$ and the mapping matrix of the conventional interpolation array B using (8) and the least squares problem (9).
5. Compute transformation matrix T in equation (10).
6. Compute the covariance matrix $\hat{\hat{\sigma}}(x,x)$ in equation (11) of the virtual array using the transformation matrix T in step 5.
7. Compute the weight vector w, equation (24), but using variance of step 6- $\hat{\hat{\sigma}}(x,x)$.
8. Compute the output array system $y_i(t)$, equation (23)
9. while $w.a(\hat{\theta}) \neq 1$
  do Minimize the output power, equation (22),
  Subject to $w.a(\hat{\theta}) = 1$,
10. Compute MVDR array interpolation spectrum for NLA, equation (26)

5.2 MUSIC Algorithm

5.2.1 MUSIC Co-prime NLA

For MUSIC, an estimate $\sigma(x,x)$ of the covariance matrix is obtained and its eigenvectors decomposed into orthogonal signal and noise subspace (Tan et al., 2014; Li et al., 2019), where the DOA is estimated from one of these subspaces. The algorithm searches through the set off all possible steering vectors to find the ones orthogonal to the noise subspace. The diagonal covariance matrix $\hat{\sigma}(x,x)$given by equation (7) is vectorized into

$$\hat{\sigma}(x,x) = Q\Lambda Q^H, \tag{27}$$

where Q is a unitary matrix containing the eigenvectors and a diagonal matrix $\Lambda = diag\{\lambda_1, \lambda_2 \ldots \lambda_K\}$, of real eigenvalue ordered as $\lambda_1 \geq \lambda_2 \geq \cdots \geq \lambda_K \geq 0$. The vector that is orthogonal to A is the eigenvector of R having the eigenvalues of Λ. The MUSIC spatial spectrum is defined by

$$P_{MUSIC_{Co-Prime}}(\hat{\theta}) = \frac{1}{\mathrm{a}^{\mathrm{H}}(\hat{\theta})\mathrm{Q_n}\mathrm{Q_n^H}\mathrm{a}(\hat{\theta})}, \tag{28}$$

where $a(\hat{\theta})$ is the steering vector corresponding to one of the incoming signals and $\mathrm{Q_n}$ is the noise subspace of the eigenvectors. The MUSIC technique for co-prime array is summarized in Algorithm 3.

Algorithm 3: MUSIC Algorithm using co-prime

1. Input: $x = \{x_i(t)\} = f(\alpha_i, \hat{\theta}_i)$, M, N, L, K, d, λ, Z and $\mu \leftarrow$ Step size
2. Compute covariance matrix $\hat{\sigma}(x, x)$equation (7)
3. Decompose $\hat{\sigma}(x, x)$into eigenvectors and eigenvalues in equation (27)
4. Rearrange the eigenvectors and eigenvalues into the signal subspace and noise subspace
5. Compute the co-prime array MUSIC spectrum equation (28) by spanning $\hat{\theta}$ to acquire estimates of the angle of arrival
6. Determine the substantial peaks of $P_{MUSIC_{Co-Prime}}(\hat{\theta})$to acquire estimates of the angle of arrival

5.2.2 MUSIC Interpolation NLA

The autocorrelation matrix is decomposed into signal and noise subspaces. From (11) the covariance matrix $\hat{\hat{\sigma}}(x, x)$ is decomposed as (Li et al., 2014):

$$\hat{\hat{\sigma}}(x, x) = U_S \textstyle\sum_S U_S^H + U_N \textstyle\sum_N U_N^H, \tag{29}$$

where U_S represents the signal subspace, U_N represents the noise subspace; $\sum_S = diag\{\lambda_1, \lambda_2, \ldots, \lambda_M\}$ is the signal eigenvalue; $\sum_N = diag\{\lambda_{M+1}, \lambda_{M+2}, \ldots, \lambda_N\}$is the noise eigenvalue. The noise subspace $\sum_N$ is orthogonal to all M signal steering vectors. The spectrum of the MUSIC, algorithm is given by

$$P_{MUSIC\_AI}(\hat{\theta}) = \frac{1}{a^H(\hat{\theta}) U_N U_N^H a(\hat{\theta})} = \frac{1}{\|U_N^H a(\hat{\theta})\|}.$$
(30)

If $\hat{\theta}$ is equal to DOA, the noise subspace U_N is orthogonal to the signal steering vectors and $\left\|U_N^H a(\hat{\theta})\right\|$ becomes zero when $\hat{\theta}$ is a signal direction and the denominator is identical to zero. It is obvious that in practice, $U_N^H a(\hat{\theta}) \neq 0$ due to finite samples. If this happens, the performance of MUSIC algorithm will not be optimal.

The MUSIC technique using array interpolation is summarized in Algorithm 4.

Algorithm 4: MUSIC Algorithm using array interpolation

1. Input: $x = \{x_i(t)\} = f(\alpha_i, \hat{\theta}_i)$, M, N, L, K, d, λ, Z and $\mu \leftarrow$ Step size
2. Determine the ULA array manifold $A(\hat{\theta})$
3. Compute the real array covariance matrix $\hat{\sigma}(x,x)$ equation (7)
4. Compute the virtual array manifold $\bar{A}(\hat{\theta})$ and the mapping matrix of the conventional interpolation array B using (8) and the least squares problem (9).
5. Compute transformation matrix G in equation (10).
6. Compute the covariance matrix $\hat{\bar{\sigma}}(x,x)$ in equation (11) of the virtual array using the transformation matrix G in step 5.
7. Decompose $\hat{\bar{\sigma}}(x,x)$ into eigenvectors and eigenvalues in equation (29)
8. Rearrange the eigenvectors and eigenvalues into the signal subspace and noise subspace.
9. Compute MUSIC array interpolation spectrum for NLA, equation (30) by spanning $\hat{\theta}$ to acquire estimates of the angle of arrival
10. Determine the substantial peaks of $P_{MUSIC_AI}(\hat{\theta})$to acquire estimates of the angle of arrival.

5.3 A-MUSIC Algorithm

5.3.1 A-MUSIC Co-prime NLA

The existing MVDR and MUSIC algorithms are adversely affected by the low SNR in rain-impacted systems and need modifications. The A-MUSIC algorithm (Nxumalo et al., 2019) repeatedly reconstructs the covariance matrix to obtain two noise and signal subspaces continuously that are averaged for several iterations mitigating against the low SNR effects. From (7), the covariance matrix $\tilde{\sigma}(x,x)$ is reconstructed as

$$\tilde{\sigma}(x,x) = \hat{\sigma}(x,x) + J\hat{\sigma}(x,x)^{*}J, \tag{31}$$

where J is MATLAB constructions given as $J = fliplr(eye(L))$ which returns columns flipped in the left-right direction and L is the number of elements. The eigen decomposition on reconstructed covariance matrix $\tilde{\sigma}(x,x)$ is

$$\tilde{\sigma}(x,x) = \hat{Q}\Lambda\hat{Q}^{H} = Q_{S1}\Lambda_{S1}Q_{S1}^{H} + Q_{N1}\Lambda_{N1}Q_{N1}^{H}, \tag{32}$$

where $\tilde{\sigma}(x,x)$ is divided into signal subspace Q_S and noise subspace Q_N. Using low rank of matrix instead of full rank matrix, $\tilde{\sigma}(x,x)$ can be reconstructed into ω_x as

$$\omega_x = Q_{S2}\Lambda_{S2}Q_{S2}^{H} + Q_{N2}\Lambda_{N2}Q_{N2}^{H}. \tag{33}$$

The average signal subspace, signal eigenvalue, noise subspace, and the noise eigenvalue are given by

$$Q_S = \frac{(Q_{S1}+Q_{S2})}{2}, \; Q_N = \frac{(Q_{N1}+Q_{N2})}{2},$$

$$\Lambda_S = \frac{(\Lambda_{S1}+\Lambda_{S2})}{2}, \Lambda_N = \frac{(\Lambda_{N1}+\Lambda_{N2})}{2} \tag{34}$$

The A-MUSIC spectrum is then defined by

$$P_{Advanced-MUSIC}(\hat{\theta}) = \frac{a^H(\hat{\theta})\left[\frac{\left(\breve{\sigma}(s,s)\breve{\sigma}(s,s)^H\right)}{K}\right]a(\hat{\theta})}{a^H(\hat{\theta})\breve{\sigma}(n,n)a(\hat{\theta})}, \tag{35}$$

where $\breve{\sigma}(s,s) = Q_S\Lambda_S^{-1}Q_S^H$, and $\breve{\sigma}(n,n) = Q_N\Lambda_N^{-1}Q_N^H$ are signal and noise subspace covariance matrix. The A-MUSIC technique using co-prime array is summarized in algorithm 5.

Algorithm 5: Proposed A-MUSIC Algorithm using co-prime array

1. **Input:** $x = \{x_i(t)\} = f(\alpha_i, \hat{\theta}_i)$, M, N, L, K, d, λ, Z and $\mu \leftarrow$ Step size
2. Compute the covariance matrix $\hat{\sigma}(x,x)$, equation (7)
3. Compute reconstructed covariance matrix $\tilde{\sigma}(x,x)$, equation (31)
4. Compute the eigen decomposition on reconstructed covariance matrix $\tilde{\sigma}(x,x)$, equation (32)
5. Compute reconstructed covariance matrix ω_x in equation (33)
6. Compute the average signal subspace, noise subspace, signal eigenvalues, and the noise eigenvalue, Q_S, Q_N, Λ_S, Λ_N in equation (34)
7. Determine signal and noise subspace averaged covariance matrix $\breve{\sigma}(s,s)$, $\breve{\sigma}(n,n)$
8. Compute the spectrum function, equation (35) spanning $\hat{\theta}$.

5.3.2 A-MUSIC Interpolation NLA

In A-MUSIC array interpolation, we reconstruct the decomposed autocorrelation matrix into signal and noise subspaces. Using equation (11), the reconstructed covariance matrix $\vec{\sigma}(x,x)$ can be written as

$$\vec{\sigma}(x,x) = \hat{\hat{\sigma}}(x,x) + J\hat{\hat{\sigma}}(x,x)^*J, \tag{36}$$

with $\hat{\hat{\sigma}}(x,x)$ the covariance matrix of equation (29). The eigen decomposition on reconstructed covariance matrix $\vec{\sigma}(x,x)$ is

$$\vec{\sigma}(x,x) = \hat{\Phi}\Pi\hat{\Phi}^H = \Phi_{S1}\Pi_{S1}\Phi_{S1}^H + \Phi_{N1}\Pi_{N1}\Phi_{N1}^H, \tag{37}$$

where $\vec{\sigma}(x,x)$ is divided into signal subspace Φ_S and noise subspace Φ_N. Using low rank of matrix instead of full rank matrix, $\vec{\sigma}(x,x)$ can be reconstructed into ϖ_x as

$$\varpi_x = \Phi_{S2}\Pi_{S2}\Phi_{S2}^H + \Phi_{N2}\Pi_{N2}\Phi_{N2}^H. \tag{38}$$

The average signal subspace, signal eigenvalue, noise subspace, and the noise eigenvalue are given by

$$\Phi_S = \frac{(\Phi_{S1}+\Phi_{S2})}{2}, \ \Phi_N = \frac{(\Phi_{N1}+\Phi_{N2})}{2},$$

$$\Pi_S = \frac{(\Pi_{S1}+\Pi_{S2})}{2}, \Pi_N = \frac{(\Pi_{N1}+\Pi_{N2})}{2} \tag{39}$$

The A-MUSIC spectrum is then defined by

$$P_{Advanced-MUSIC}(\hat{\theta}) = \frac{a^H(\theta)\left[\frac{\left(\vec{\sigma}(s,s)\vec{\sigma}(s,s)^H\right)}{I}\right]a(\hat{\theta})}{a^H(\hat{\theta})\,\vec{\sigma}(n,n)a(\hat{\theta})}, \tag{40}$$

where $\vec{\sigma}(s,s) = \Phi_S \Pi_S^{-1} \Phi_S^H$, and $\vec{\sigma}(n,n) = \Phi_N \Pi_N^{-1} \Phi_N^H$ are signal and noise subspace covariance matrix. The A-MUSIC technique is summarized in Algorithm 6.

Algorithm 6: Proposed A-MUSIC Algorithm using array interpolation

1. Input: $x = \{x_i(t)\} = f(\alpha_i, \hat{\theta}_i)$, M, N, L, K, d, λ, Z and $\mu \leftarrow$ Step size
2. Determine the ULA array manifold $A(\hat{\theta})$
3. Compute the real array covariance matrix $\hat{\sigma}(x,x)$ equation (7)
4. Compute the virtual array manifold $\bar{A}(\hat{\theta})$ and the mapping matrix of the conventional interpolation array B using (8) and the least squares problem (9).
5. Compute transformation matrix G in equation (10).
6. Compute the covariance matrix $\hat{\hat{\sigma}}(x,x)$ in equation (11) of the virtual array using the transformation matrix G in step 5.
7. Compute reconstructed covariance matrix $\vec{\sigma}(x,x)$ equation (36)
8. Decompose $\vec{\sigma}(x,x)$ into eigenvectors and eigenvalues, equation (37)
9. Compute the average signal subspace, noise subspace, signal eigenvalues, and the noise eigenvalue Φ_S, Φ_N, Π_S, Π_N, equation (39)
10. Determine signal and noise subspace averaged covariance matrix $\vec{\sigma}(s,s)$, $\vec{\sigma}(n,n)$
11. Compute the spectrum function $P_{Advanced-MUSIC}(\hat{\theta})$ spanning $\hat{\theta}$ equation (40).

---

6 Performance Measures

6.1 Root Mean Square Error (RMSE)

The performance of the DOA estimation algorithms is evaluated in terms of algorithms spectrum functions, equations (25), (26), (28), (30), (35) and (40), the Root Mean Square Error (RMSE) and the signal to noise ratios. The RMSE is given by

$$RMSE = \sqrt{\frac{1}{Z*K}\sum_{j=1}^{Z}\sum_{i=1}^{K}(\tilde{\theta}_{ij} - \theta_i)^2}, \tag{41}$$

where Z is the number of simulation trials, K is the narrowband electromagnetic wave sources impinging upon the array and the estimate of the i^{th} angle of arrival in the j^{th} trial is $\tilde{\theta}_{ij}$. Where utilised, the signal to noise ratio (SNR) is given by

$$SNR = 20\log_{10}\left(\frac{x}{v}\right), \tag{42}$$

where x is the received signal strength in dB and v is the noise strength in dB. The overall performance evaluation is done as in algorithm 7.

Algorithm 7: System Algorithm

1. Choose an event
2. Compute expected rain rate, equation (16)
Compute the actual rain rate r from lognormal distribution with given mean
3. **for** i number of antennas $< L_{max}$
4. Compute the rain attenuation α_r, total attenuation A_T and angle $\hat{\theta}_i$.
Determine the angle deviation $\Delta\theta_i$, equation (20) and the mean μ_θ.
5. **end for**
6. Determine the received signal $x_i(t)$.
7. Compute DOA, algorithms 1, 2, 3, 4, 5 and 6.

6.2 Cramer Rao Bound (CRB)

To validate our DOA estimators, the Cramer Rao Bound (CRB) which shows the limit that can be achieved by an unbiased estimator is applied. The general CRB formula for the case of multiple DOA parameters per source and spatially uncorrelated white noise is developed in (Nehorai et al., 1994). The following compact matrix expression for the stochastic CRB was derived in (Stoica et al., 1990) and is applied in our case with the few required modification,

$$CRB = \frac{\sigma^2}{2T}\left(Re\{H \odot G^T\}\right)^{-1}, \tag{42}$$

where T is the number of data snapshots, $H = D^H[I - A(A^HA)^{-1}A^H]D$, $G = \sigma(s,s)A^H(\sigma(x,x))^{-1}A\sigma(s,s)$, $D = [d(\theta_1), \dots, d(\theta_K)]$, $d(\theta_i) = {da(\theta)}/{d\theta}\,|_{\theta=\theta_i}$, $\sigma(x,x) = E[x(t)x^H(t)] = A\sigma(s,s)A^H + \vartheta^2 I$, $\sigma(s,s) = E[s(t)s^H(t)]$, I is the identity matrix, ϑ^2 is the noise variance, and $E\{\cdot\}$ denotes the expectation.

6.3 DOA Estimation Algorithm complexity

The complexity of MVDR and MUSIC algorithm has been derived and shown in Table 2 (Meng et al., 2019). For A-MUSIC, there are three major computational steps needed to estimate the DOA. The complexity of the first step is the covariance function and reconstruction of the covariance matrix, $\mathcal{O}(L^2K)$. The second step is the eigenvalue decomposition operation, which has a complexity of $\mathcal{O}(L^3)$. The third step is obtaining the spatial pseudo spectrum, which has a complexity of $\mathcal{O}(J_\theta . J_{\Delta\theta}(L+1)(L-K)/2)$, with J being the number of spectral points of the total angular field of view. Therefore, the total complexity of A-MUSIC is given by $\mathcal{O}(L^2K + L^3) + \mathcal{O}(J_\theta . J_{\Delta\theta}(L+1)(L-K)/2)$.

Note that the complexity of deriving the covariance matrix for co-prime and array interpolation, and the complexity of deriving the weather effectors is same for all the algorithms and is not included in the derivation.

Table 2. Computational Complexities of DOA Estimation Algorithms.

DOA algorithm	**Computational Complexity**
MVDR	$\mathcal{O}(L^2K + L^3 + (2L^2 + 3L))$
MUSIC	$\mathcal{O}(L^2K + L^3 + JL)$
A-MUSIC	$\mathcal{O}(L^2K + L^3) + \mathcal{O}(J_\theta . J_{\Delta\theta}(L+1)(L-K)/2)$

7 Simulation Results

An investigation into the performance of MVDR, MUSIC and the proposed A-MUSIC DOA algorithms for NLA is presented in this section. The performance investigation is based on co-prime array and array interpolation methods of a pair of sparse NLAs for different number of array elements, rain rates and SNR. The developed results are for a case where signals impinge on the NLA sensors from the same signal source. It is assumed that the signals are mutually independent and that noise is additive white Gaussian noise (AWGN) with a zero mean. Unless explicitly stated, the simulation parameters are as in Table 3.

Table 3. Simulation parameters

MVDR, MUSIC AND A-MUSIC	
Simulation parameters	**Values**
Input θ	5^0, 25^0, 45^0, 65^0
Number of elements L	10
Spacing difference	$d = \lambda/_2 * [0,3,5,6,9,10,12,15,20,25]$
Signal-to-noise ratio	SNR = 20dB
Number of Snapshots	Z = 300
Rain rate in (mm/hr) [no rain, drizzle rain, widespread rain, shower rain, thunderstorm]	[0, 2.5, 6, 15, 40]
α at f = 80 GHz	0.7103
k at f = 80 GHz	1.16995
$\Delta\theta_{min}, \Delta\theta_{max}$	$[0^0 - 60^0]$
M, N,	3, 5

The results of Fig. 6(a)-6(d) and Fig. 7(a)-6(d) show co-prime array and array interpolation based spatial output spectrum of the MVDR, MUSIC and the proposed A-MUSIC for different rain rates; no rain, widespread, shower and thunderstorm rain conditions. Note that without rain, the spectrum results for MVDR and MUSIC are similar to the ones in (Tan et al., 2014, Li et al., 2019) respectively. From the results, the following can be observed, the accuracy of DOA estimation reduces with increasing rain rate due to the high signal distortion at higher rain rates. The performance of the A-MUSIC is better than MUSIC followed by MVDR. This is because of the multiple averaging nature of the A-MUSIC algorithm. It can further be observed that at higher rain rates in the thunderstorm events, MVDR and MUSIC do not estimate the direction of arrival accurately.

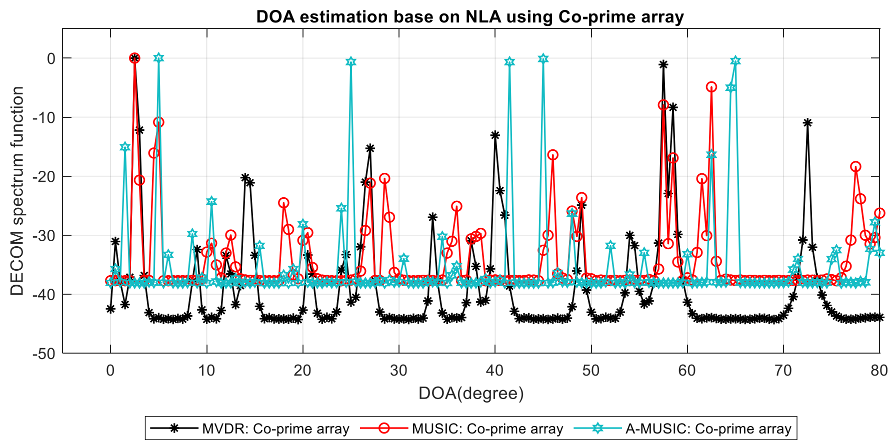

Figure 6: (a) DOA estimation attenuation using Co-prime array with no rain

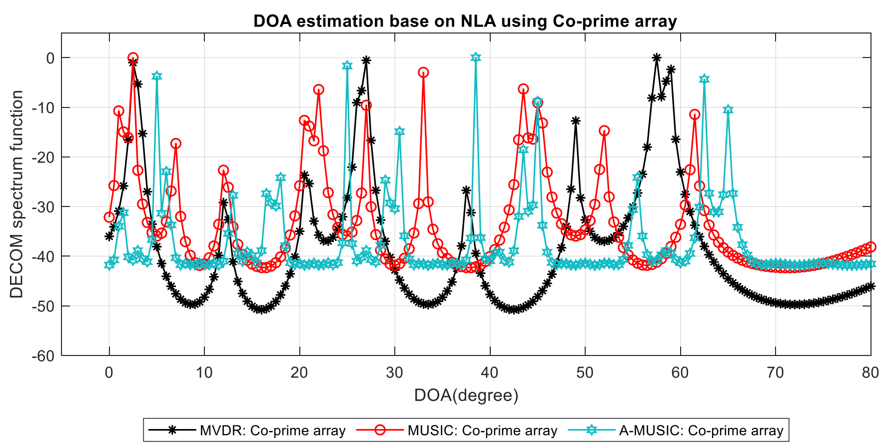

Figure 6: (b) DOA estimation attenuation using Co-prime array for widespread rainfall

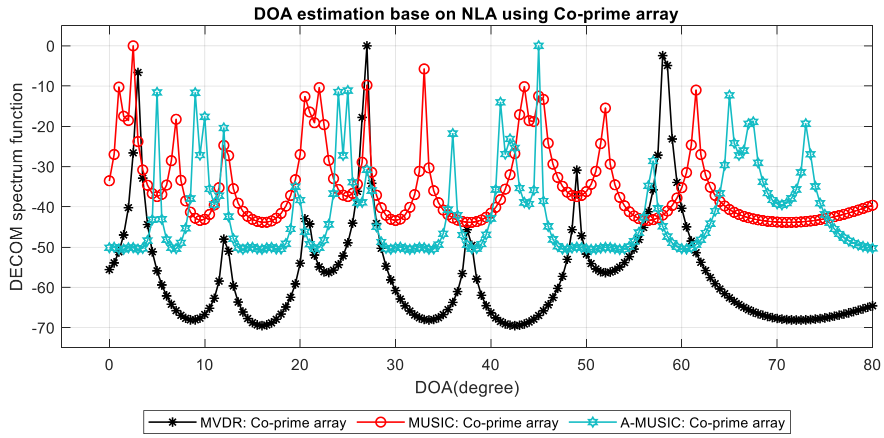

Figure 6: (c) DOA estimation attenuation using Co-prime array for shower rainfall

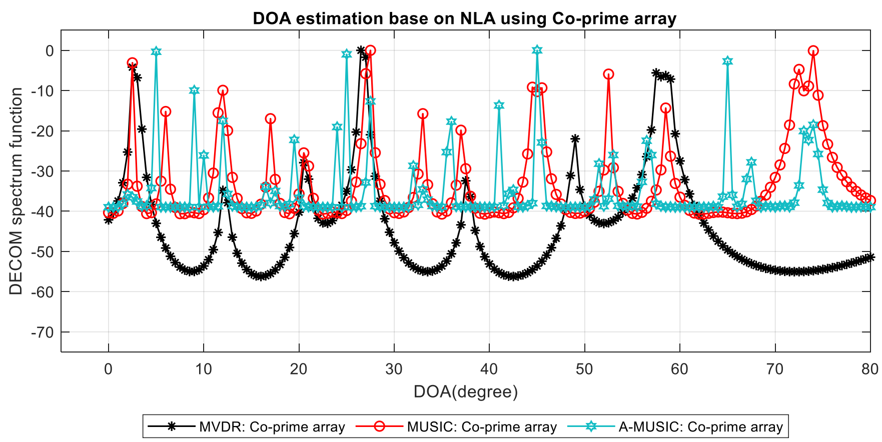

Figure 6: (d) DOA estimation attenuation using Co-prime array for thunderstorm rainfall

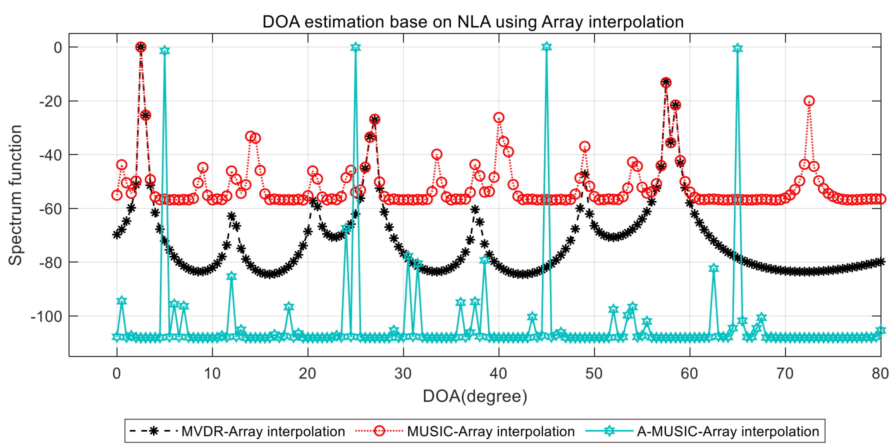

Figure 7: (a) DOA estimation attenuation using array interpolation with no rain

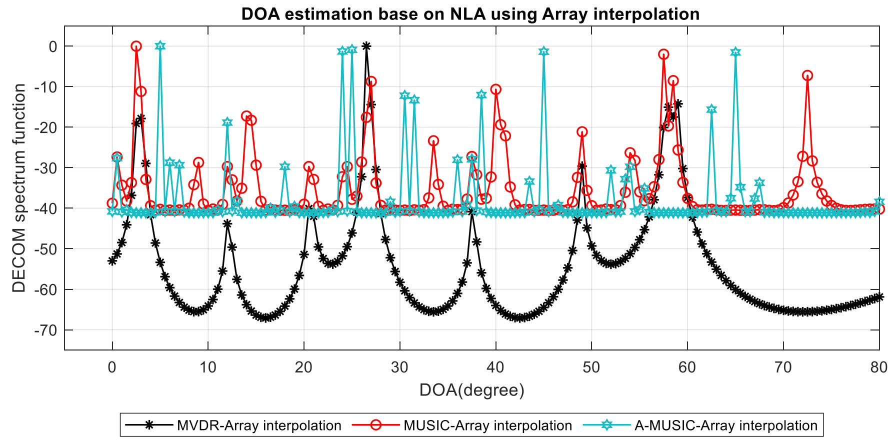

Figure 7: (b) DOA estimation attenuation using array interpolation for widespread rainfall

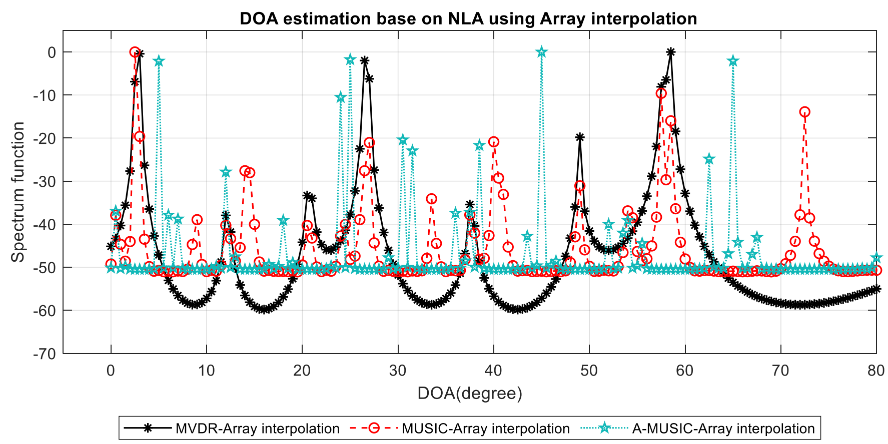

Figure 7: (c) DOA estimation attenuation using array interpolation for shower rainfall

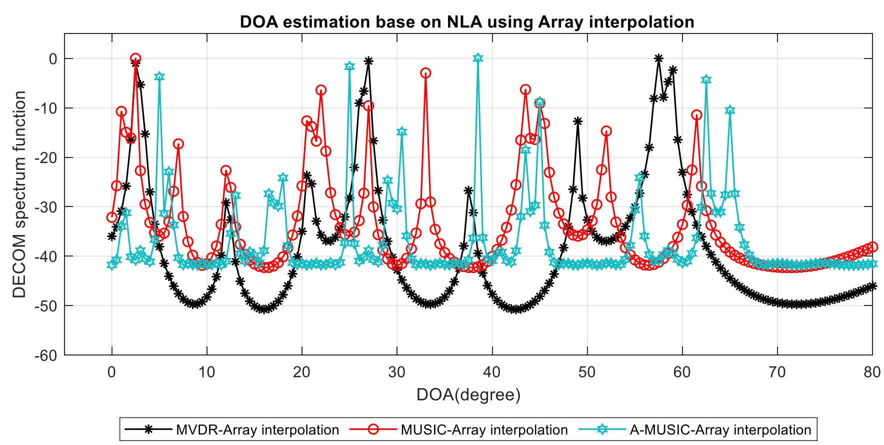

Figure 7: (d) DOA estimation attenuation using array interpolation for thunderstorm rainfall

The results of Fig. 8(a)-8(c) represent the RMSE value vs rain rate comparison of co-prime array and array interpolation of DOA algorithms for different number of elements. As expected, the RMSE increases with increasing rain rates while the error reduces with an increase in the number of antenna elements. A noticeable difference in performance is when the rain rate exceeds 10 mm/hr. It can also be observed that the co-prime array configuration results in a higher error than the array interpolation method.

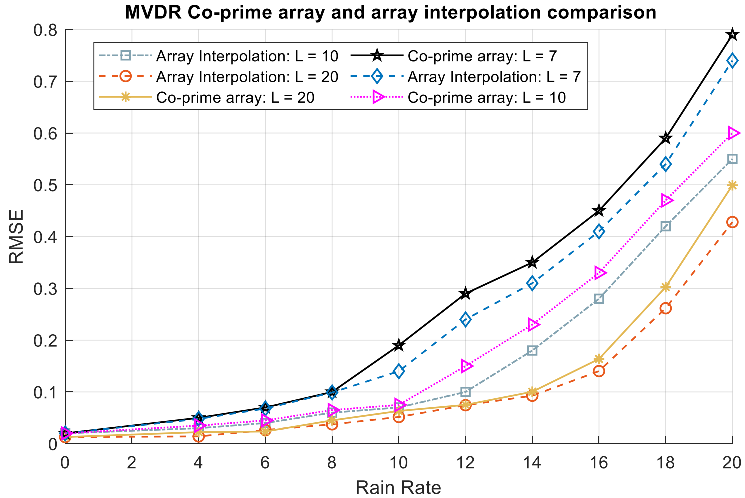

Figure 8(a): MVDR RMSE vs rain rate for coprime and array interpolation at *L*=7, 10, 20

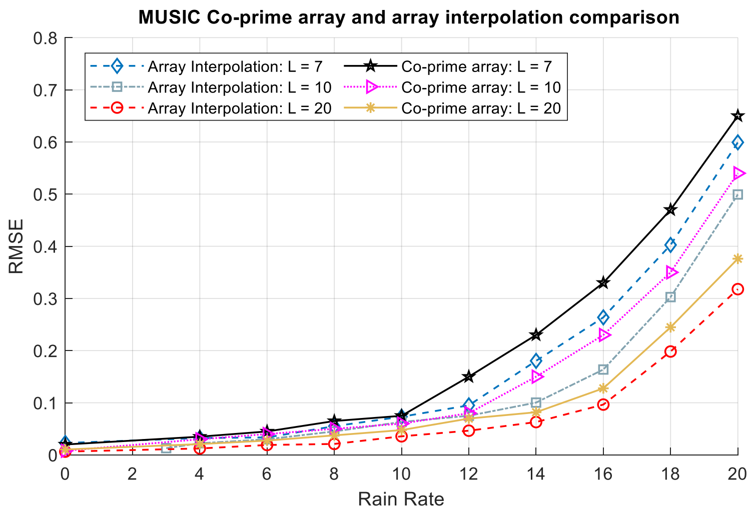

Figure 8(b): MUSIC RMSE vs rain rate for coprime and array interpolation at *L*=7, 10, 20

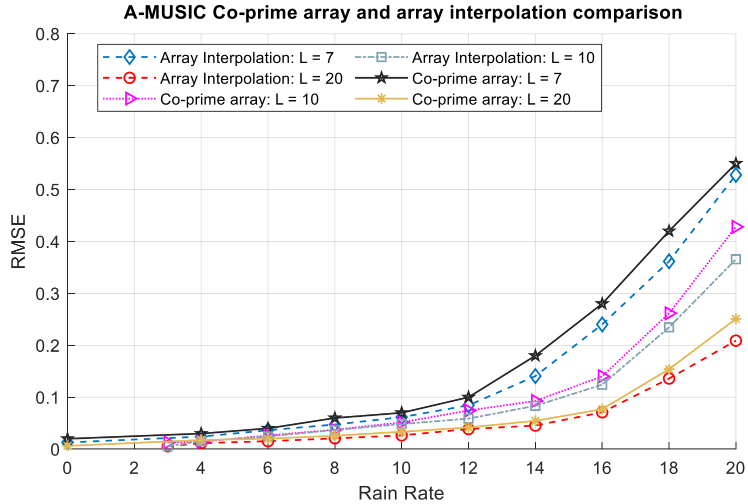

Figure 8(c): A-MUSIC RMSE vs rain rate for coprime and array interpolation at L=7, 10, 20

The results of Fig. 9(a)–(c) represent a comparison of the three DOA algorithms for different rain rates at different antenna elements. As observed above, the RMSE increases with increase in rainfall and reduction in number of antenna elements. The proposed A-MUSIC performs better than MUSIC and MVDR in that order. This can be attributed to the repeated reconstruction of the covariance matrix to obtain two noise and signal subspaces continuously that are averaged for several iterations.

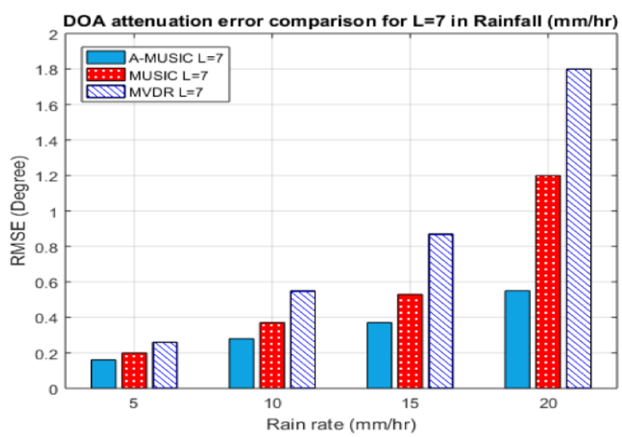

(a)

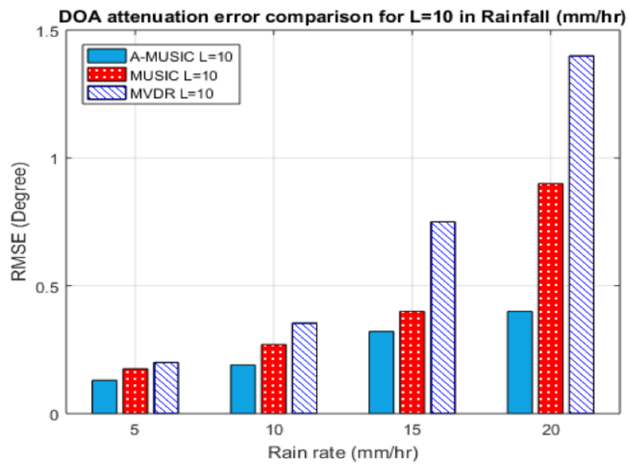

(b)

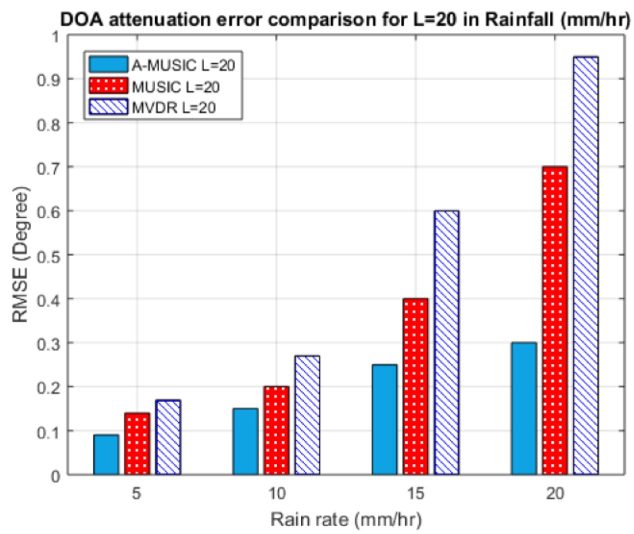

(c)

Figure 9: DOA estimation attenuation error comparison. (a) DOA estimation attenuation error comparison for L = 7. (b) DOA estimation attenuation error comparison for L = 10. (c) DOA estimation attenuation error comparison for L = 20.

The performance of the system is investigated further at different SNR conditions for a co-prime configuration in Fig. 10 and array interpolation in Fig. 11. At r = 10 mm/hr. It is observed that as the SNR increases, the RMSE decreases. The A-MUSIC co-prime array-based algorithm outperforms the MVDR and MUSIC algorithm, and its performance trend is within the CRB bounds. This demonstrates that the proposed method can still achieve satisfactory performance at lower SNR conditions.

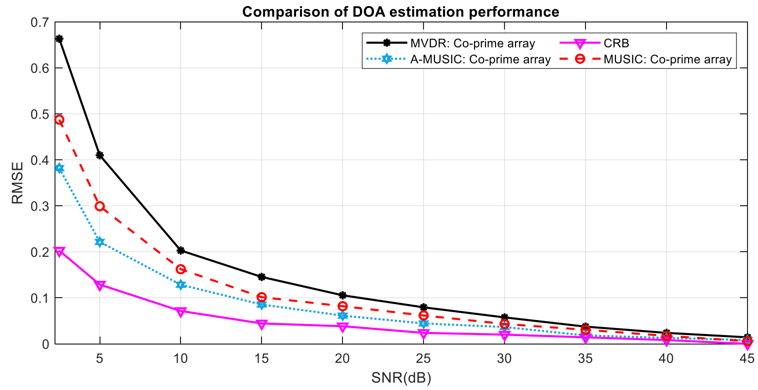

Figure 10: DOA estimation using co-prime array error comparison vs SNR

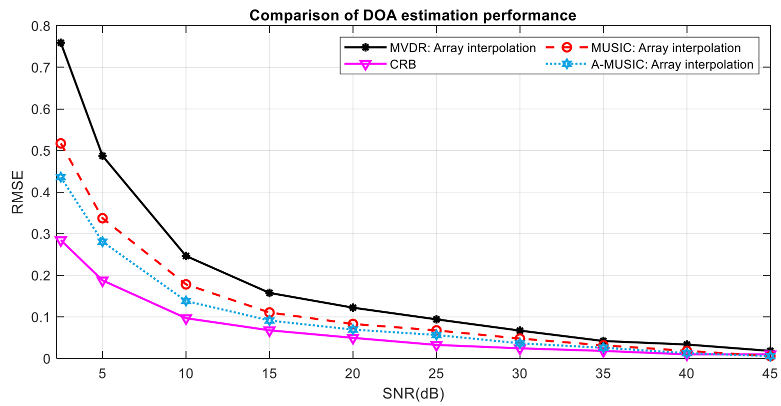

Figure 11: DOA estimation using array interpolation error comparison vs SNR

In Fig. 12, the systems error performance at various number of snapshots is presented for condition where r = 10 mm/hr and SNR = 20dB. As expected, the RMSE decreases as we increase the number of trials from 100 to 500. Therefore, this shows that by increasing the number of simulation trials, the algorithm's performance can be greatly improved. Furthermore, one can intuitively observe that the performance of the proposed A-MUSIC surpasses the classical MUSIC and the MVDR estimator over the range of the number of snapshots simulated.

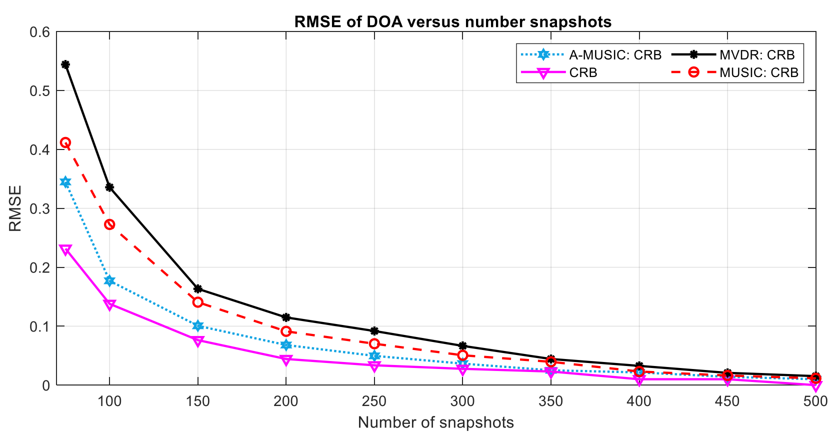

Figure 12: DOA estimation CRB error comparison vs number of snapshots

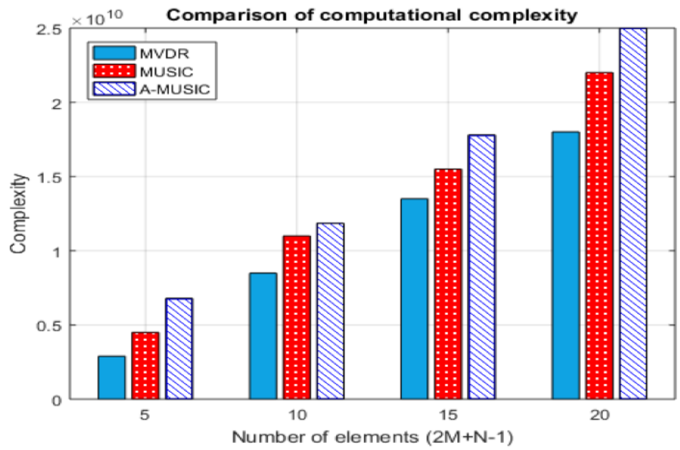

Figure 13: Comparison of computational complexity

In Fig. 13, the computational complexity of A-MUSIC and the other DOA estimation algorithms is compared at different antenna elements. Although A-MUSIC algorithm have high performance in estimating the DOA, its computational complexity is high compared to MVDR and MUSIC estimations. This is because of the multiple averaging nature of A-MUSIC algorithm.

8 Conclusions

This work has investigated and evaluated the performance of DOA algorithms for non-uniform linear arrays (NLA) in weather-impacted environment. The investigation is conducted with no rain, widespread, shower and thunderstorm rainfall events. From the investigation, the algorithm's performance accuracy significantly reduce from no rain condition to thunderstorm rainfall condition with MUSIC performing better than MVDR. In terms of RMSE, the algorithm's performance decline as the SNR values and number of snapshots are increased. The work develops an A-MUSIC algorithm for the weather impacted conditions in NLA. The performance of the developed A MUSIC is superior to the existing algorithm in terms of accuracy and RMSE parameters. This work opens further investigation of performance of DOA algorithms in weather-impacted environment and the need for a re-design of the existing algorithms. The accuracy of the investigated algorithms needs to be validated further while considering other statistical, analytical and computational measures.

References

Krim, H., Viberg, M. (1996), Two decades of array signal processing research: the parametric approach, *IEEE Signal Processing Magazine*, vol.13, (4), pp. 67- 94.

El Kassis, C., Picheral, J., Mokbel, C. (2010), Advantages of nonuniform arrays using root-MUSIC. *Signal Process*. 90(2), 689–695.

Saric, Z., Kukolj, D., Teslic, N. (2010), Acoustic source localization in wireless sensor network. Circuits Syst. *Signal Process*. 29, 837–856.

Schmidt, R.O. (1986), Multiple emitter location and signal parameter estimation, *IEEE Trans. Antennas Propag.*, vol. 34, no. 3, pp. 276–280.

Vaidyanathan, P. P., and Pal, P. (2011), Sparse sensing with co-prime samplers and arrays, *IEEE Transactions on Signal Processing*, vol. 59, no. 2, pp. 573–586.

Tan, Z., Nehorai, A., and Eldar, Y. C. (2014), Continuous sparse recovery for direction of arrival estimation with co-prime arrays, *2014 IEEE 8th Sensor Array and Multichannel Signal Processing Workshop (SAM)*, A Coruna, pp. 393-396.

Li, W., Mao, X., Yu, W., and Yue, C. (2014), An Effective Technique for Enhancing Direction Finding Performance of Virtual Arrays, International Journal of Antennas and Propagation, vol. 2014, Dec. 2014.

Choi, Y. H., (2010), ESPRIT-based coherent source localization with forward and backward vectors, *IEEE Transactions on Signal Processing*, vol. 58, (12), pp. 67-94.

Moffet, A. (1968), Minimum-redundancy linear arrays, *IEEE Trans. Antennas Propag.*, vol. AP-16, no. 2, pp. 172–175, Mar. 1968.

Bloom, G. S., and Golomb, S. W. (1977), Application of numbered undirected graphs," *Proc. IEEE*, vol. 65, no. 4, pp. 562–570, Apr. 1977.

Pal, P., and Vaidyanathan, P. P. (2010), Nested Arrays: A Novel Approach to Array Processing with Enhanced Degrees of Freedom, in *IEEE Transactions on Signal Processing*, vol. 58, no. 8, pp. 4167-4181, Aug. 2010, doi: 10.1109/TSP.2010.2049264.

Pal, P., and Vaidyanathan, P. P. (2011), Coprime sampling and the MUSIC algorithm, in IEEE Digital Signal Process. *Workshop and IEEE Signal Process*. Education Workshop, Sedona, AZ, 2011, pp. 289–294.

Bronez, T. P. (1988), Sector interpolation of non-uniform arrays for efficient high resolution bearing estimation, ICASSP-88., *International Conference on Acoustics, Speech, and Signal Processing*, New York, NY, USA, pp. 2885-2888 vol.5, doi: 10.1109/ICASSP.1988.197256.

Friedlander, B. (1993), The root-music algorithm for direction finding with interpolated arrays, *Signal Process.*, 30(1), 15–29.

Friedlander, B., and Weiss, A. J. (1992), Direction finding using spatial smoothing with interpolated arrays, *IEEE Trans. Aerosp. Electron. Syst*., vol. 28, pp. 574–587, Apr. 1992.

Friedlander, B., and Weiss, A. J. (1993), Direction finding for wideband signals using an interpolated array, *IEEE Trans. Signal Process.*, vol. 41, pp. 1618–1634, Apr. 1993.

Weiss, A. J., Friedlander, B., and Stoica, P. (1995), Direction-of-arrival estimation using MODE with interpolated arrays, *IEEE Trans. Signal Process.*, vol. 43, no. 1, pp. 296–300, Jan. 1995

Gershman, A. B., and Böhme, J. F. (1997), A note on most favorable array geometries for DOA estimation and array interpolation, *IEEE Signal Process. Lett.*, vol. 4, pp. 232–235, Aug. 1997.

Sidorovitch, D. V., and Gershman, A. B. (1998), 2-D wideband interpolated root-MUSIC applied to measured seismic data, *IEEE Trans. Signal Process.*, vol. 46, no. 8, pp. 2263–2267, Aug. 1998.

Hyberg, P., Jansson, M., and Ottersten, B. (2004), Array interpolation and bias reduction," *IEEE Trans. Signal Process.*, vol. 52, no. 10, pp. 2711–2720, Oct. 2004.

Hyberg, P., Jansson, M., and Ottersten, B. (2005), Array interpolation and DOA MSE reduction, *IEEE Trans. Signal Process.*, vol. 53, no. 12, pp. 4464–4471, Dec. 2005.

Abramovich, Y. I., Spencer, N. K., Gorokhov, A. Y. (1999), Resolving manifold ambiguities in direction-of-arrival estimation for nonuniform linear antenna arrays", *IEEE Transactions on Signal Processing*, vol.47,(10), pp.2629-2643.

Rubsamen, M., Gershman, A. B. (2009), Direction-of-arrival estimation for nonuniform sensor arrays: from manifold separation to Fourier domain MUSIC methods", *IEEE Transactions on Signal Processing*, vol.57, (2), pp.588-599.

Dai, J. S., Zhao, D., Ye, Z. F. (2010), DOA estimation and self-calibration algorithm for nonuniform linear array, In Proc. *IEEE International Symposium on Intelligent Signal Processing*, pp.1-4.

Rao, B. D., and Hari, K. V. S. (1989), Performance analysis of root-music, *IEEE Trans. Acoustic. Speech Signal Process.*,37(12), 1939–1949, doi:10.1109/29.45540.

Swindlehurst, A. L., and Kailath, T. (1992), A performance analysis of subspace-based methods in the presence of model errors. I. the MUSIC algorithm, *IEEE Trans. Acoustic. Speech Signal Process.*,40(7), 1758–1774, doi:10.1109/78.143447.

Trees, H. V. (2002), Optimum Array Processing, vol. 4, Detection, Estimation, and Modulation Theory, John Wiley, NewYork.

Wu, H. T., Yang, J., Chen, F. K. (1995), Source number estimation using transformed gerschgorin radii, *IEEE Transactions on Signal Processing*, vol. 43,(6),pp.1325-1333.

Kritchman, S., Nadler, B. (2005), Non-parametric detection of the number of signals: hypothesis testing and random matrix theory", *IEEE Transactions on Signal Processing*, vol. 57, (10), pp.3930-3941.

Fishler, E., Vincent, P. H. (2005), Estimation of the number of sources in unbalanced arrays via information theoretic criteria, *IEEE Transactions on Signal Processing*, vol. 53,(9),pp.3543-3553.

Li, X., Adal, L. (2010), Independent component analysis by entropy bound minimization, *IEEE Transactions on Signal Processing*, vol.58, (10), pp.5151-5164.

Nadler, B. (2010), Nonparametric detection of signals by information theoretic criteria: performance analysis and an improved estimator", *IEEE Transactions on Signal Processing*, vol. 58, (5), pp.2746- 2756.

Zhang, Y., Wang, P., and Goldsmith, A. (2015), Rainfall Effect on the Performance of Millimeter-Wave MIMO Systems, in *IEEE Transactions on Wireless Communications*, vol. 14, no. 9, pp. 4857-4866, Sept. 2015.

Pi, Z., and Khan, F. (2011), An Introduction to millimeter-wave mobile broadband systems, *IEEE Commun. Mag.*, vol. 49, no. 6, pp. 101–107, Jun. 2011.

Ishimaru, A., Jaruwatanadilok, S., and Kuga, Y. (2004), Multiple scattering effects on the radar cross section (RCS) of objects in a random medium including backscattering enhancement and shower curtain effects, *Waves Random Media*, vol. 14, pp. 499–511.

Agber, J. U., and Akura, J. M. (2013), A High-Performance Model for Rainfall Effect on Radio Signals. *Journal of Information Engineering and Applications*: 1-12.

Calla, O. P. N., and Purohit, J. S. (1990), Study of effect of rain and dust on propagation of radio waves at millimeter wavelength, in *Proc. URSI'90*, 1990, p. 151-155.

Zhang, Y. D., Qin, S., and Amin, M. G. (2014), DOA estimation exploiting coprime arrays with sparse sensor spacing, *2014 IEEE International Conference on Acoustics, Speech and Signal Processing (ICASSP)*, Florence, pp. 2267-2271, doi: 10.1109/ICASSP.2014.6854003.

Friedlander, B. (1990), Direction finding using an interpolated array, in *Proceedings of the International Conference on Acoustics, Speech,andSignal Processing (ICASSP '90)*, vol. 5, pp.2951–2954, Albuquerque, NM, USA, April 1990.

Tuncer, T.E., Yasar, T.K., Friedlander, B. (2007), Direction of arrival estimation for nonuniform linear arrays by using array interpolation, *Radio Sci.* 42 (4), http://dx.doi.org/10.1029/2007RS003641.

Belloni, F., Richter, A., and Koivunen, V. (2007), DOA estimation via manifold separation for arbitrary array structures, *IEEE Transactions on Signal Processing*, vol. 55, no. 10, pp. 4800–4810.

Li, W., Mao, X., Yu, W., and Yue, C. (2014), An Effective Technique for Enhancing Direction Finding Performance of Virtual Arrays, *International Journal of Antennas and Propagation*, vol. 2014, Dec. 2014.

Alonge, A.A., and Afullo, T.J. (2015), Fractal analysis of rainfall event duration for microwave and millimeter networks: rain queueing theory approach, *IET Microwaves, Antennas and Propagation*, vol. 9(4), pp. 291-300.

Kedem, B., Chiu, L. S. (1987), On the lognormality of rain rate. *Proceedings of the National Academy of Sciences*, Vol. 84, No. 4, 901-905.

Cho, H. K., Bowman, K. P., North, G. R. (2004), A comparison of gamma and lognormal distributions for characterizing satellite rain rates from the tropical rainfall measuring mission". *Journal of Applied meteorology*, Vol. 43, No. 11, 1586-1597.

I. T. U. (2005), Radio wave Propagation Series, "Specific attenuation model for rain for use in prediction methods," *Rec. P.838-3, ITU-R*, Geneva, Switzerland.

Lei Yu, Yinsheng Wei and W. Liu (2015), Adaptive beamforming based on nonuniform linear arrays with enhanced degrees of freedom, *TENCON 2015 - 2015 IEEE Region 10 Conference*, Macao, pp. 1-5, doi: 10.1109/TENCON.2015.7373099.

Tan, Z., and Nehorai, A. (2014), Sparse Direction of Arrival Estimation Using Co-Prime Arrays with Off-Grid Targets, in *IEEE Signal Processing Letters*, vol. 21, no. 1, pp. 26-29, Jan. 2014, doi: 10.1109/LSP.2013.2289740.

Li, Z., Zhou, C., Jia, Y., Wang, G., Yan, C., and Lv, Y. (2019), DOD and DOA Estimation for Bistatic Co-Prime MIMO Array Based on Correlation Matrix Augmentation, *2019 International Conference on Control, Automation and Information Sciences (ICCAIS)*, Chengdu, China, pp. 1-5, doi: 10.1109/ICCAIS46528.2019.9074651.

Nxumalo, B. P., and Walingo, T. (2019), Direction of Arrival (DOA) Estimation for Smart Antennas in Weather Impacted Environments, *Progress In Electromagnetics Research C*, Vol. 95, 209-225, 2019. doi:10.2528/PIERC19051006

Nehorai, A., and Paldi, E. (1994), Acoustic vector-sensor array processing, in *IEEE Transactions on Signal Processing*, vol. 42, no. 9, pp. 2481-2491, Sept. 1994, doi: 10.1109/78.317869.

Stoica, P., and Nehorai, A. (1990), Performance study of conditional and unconditional direction-of-arrival estimation, *IEEE Trans. Acoustic., Speech, Signal Processing*, vol. 38, pp. 1783–1795, Oct. 1990.

Meng, Z., Zhou, W. (2019), Direction-of-arrival estimation in coprime array using the ESPRIT-based method. *Sensors 19*, no. 3, 707.

Figure 1.

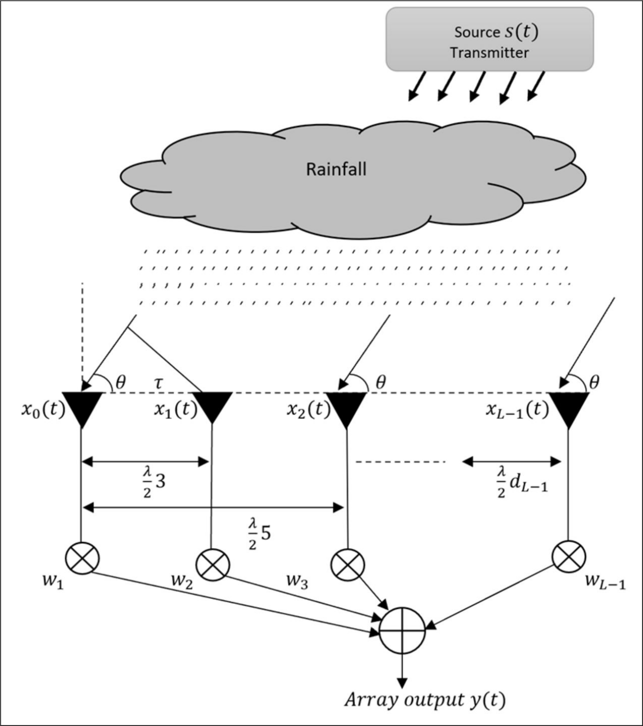

Source $s(t)$
Transmitter
Rainfall
θ
τ
θ
θ
$x_0(t)$
$x_1(t)$
$x_2(t)$
$x_{L-1}(t)$
$\frac{\lambda}{2}3$
$\frac{\lambda}{2}d_{L-1}$
$\frac{\lambda}{2}5$
w_1
w_2
w_3
w_{L-1}
Array output $y(t)$

Figure 2.

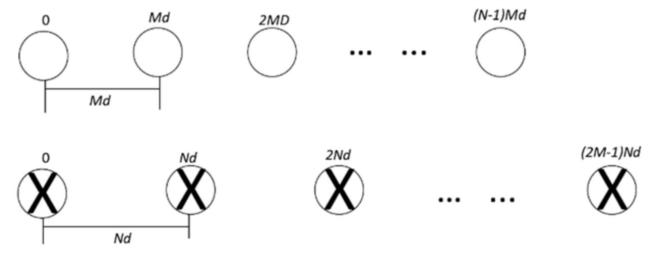

0
Md
2MD
(N-1)Md
Md
0
Nd
2Nd
(2M-1)Nd
Nd

Figure 3.

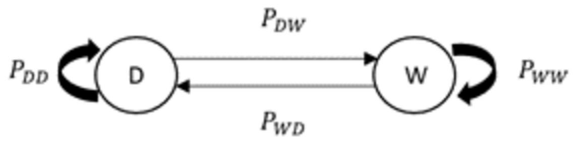
P_{DW}
P_{DD}
D
W
P_{WW}
P_{WD}

Figure 4.

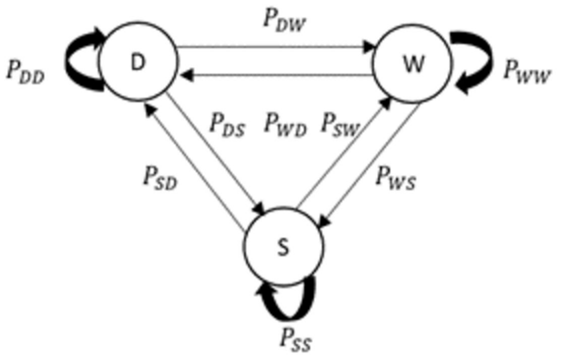

P_{DW}
D
W
P_{DD}
P_{WW}
P_{DS}
P_{WD}
P_{SW}
P_{SD}
P_{WS}
S
P_{SS}

Figure 5.

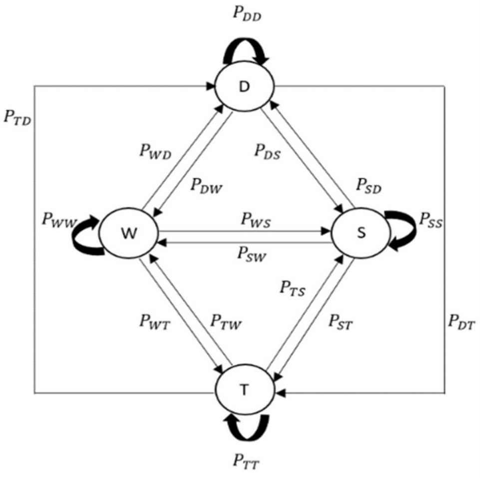

P_{DD}
D
P_{TD}
P_{WD}
P_{DS}
P_{DW}
P_{SD}
P_{WW}
W
P_{WS}
S
P_{SS}
P_{SW}
P_{TS}
P_{WT}
P_{TW}
P_{ST}
P_{DT}
T
P_{TT}

Figure 6(a).

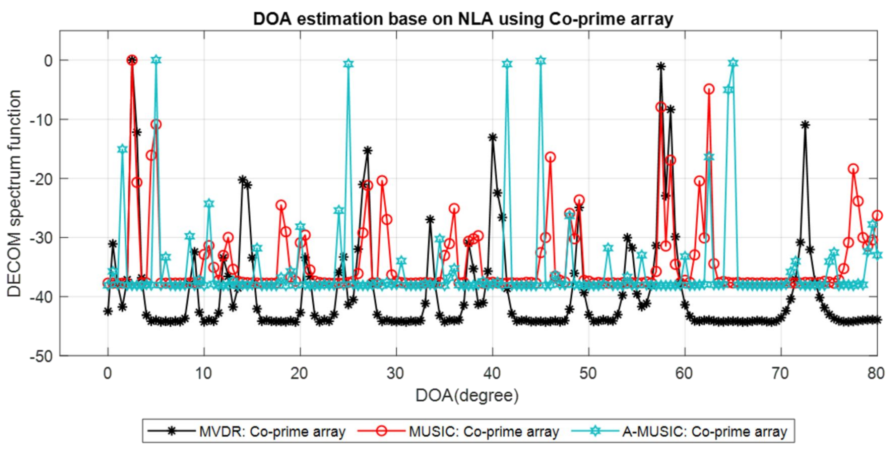
DOA estimation base on NLA using Co-prime array
DECOM spectrum function
DOA(degree)
0
-10
-20
-30
-40
-50
0
10
20
30
40
50
60
70
80
MVDR: Co-prime array
MUSIC: Co-prime array
A-MUSIC: Co-prime array

Figure 6(b).

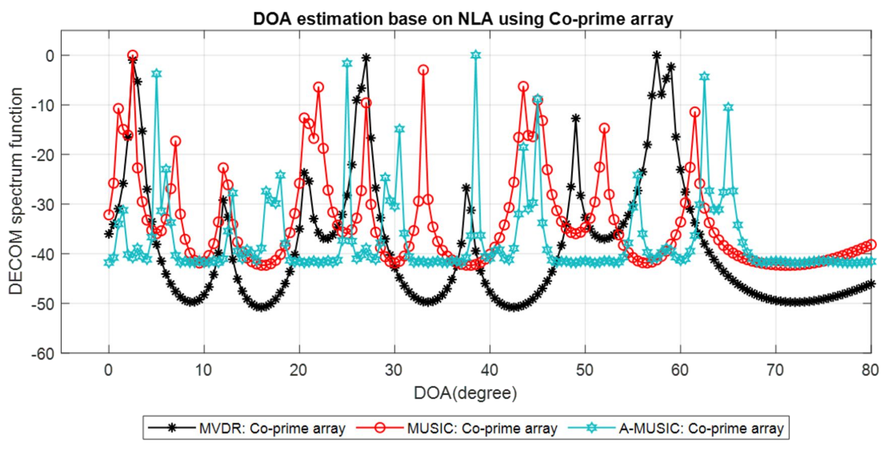
DOA estimation base on NLA using Co-prime array
DECOM spectrum function
0
-10
-20
-30
-40
-50
-60
0
10
20
30
40
50
60
70
80
DOA(degree)
MVDR: Co-prime array
MUSIC: Co-prime array
A-MUSIC: Co-prime array

Figure 6(c).

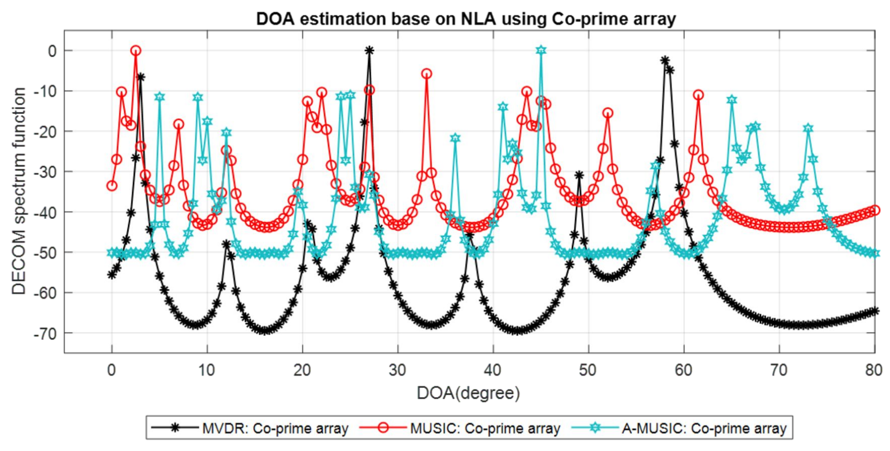

DOA estimation base on NLA using Co-prime array
DECOM spectrum function
0
-10
-20
-30
-40
-50
-60
-70
0
10
20
30
40
50
60
70
80
DOA(degree)
MVDR: Co-prime array
MUSIC: Co-prime array
A-MUSIC: Co-prime array

Figure 6(d).

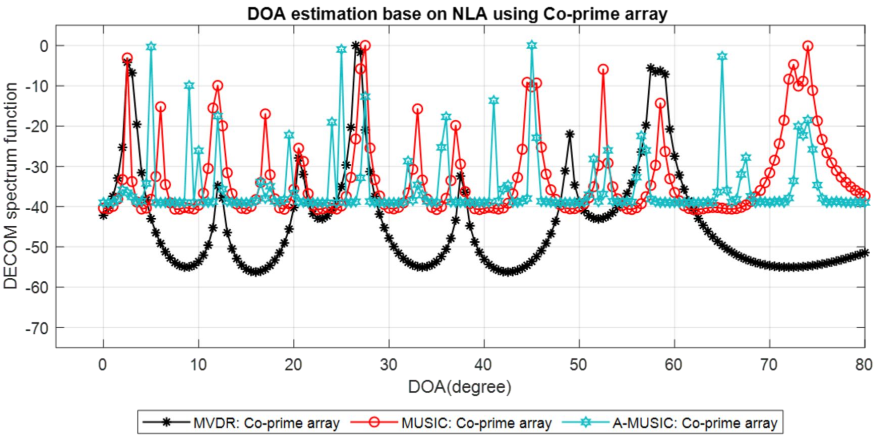
DOA estimation base on NLA using Co-prime array
DECOM spectrum function
0
-10
-20
-30
-40
-50
-60
-70
0
10
20
30
40
50
60
70
80
DOA(degree)
MVDR: Co-prime array
MUSIC: Co-prime array
A-MUSIC: Co-prime array

Figure 7(a).

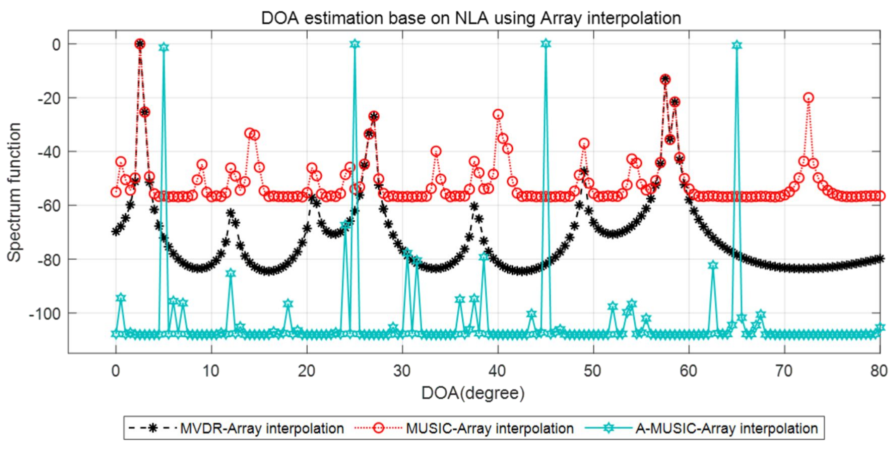

DOA estimation base on NLA using Array interpolation
Spectrum function
0
-20
-40
-60
-80
-100
0
10
20
30
40
50
60
70
80
DOA(degree)
MVDR-Array interpolation
MUSIC-Array interpolation
A-MUSIC-Array interpolation

Figure 7(b).

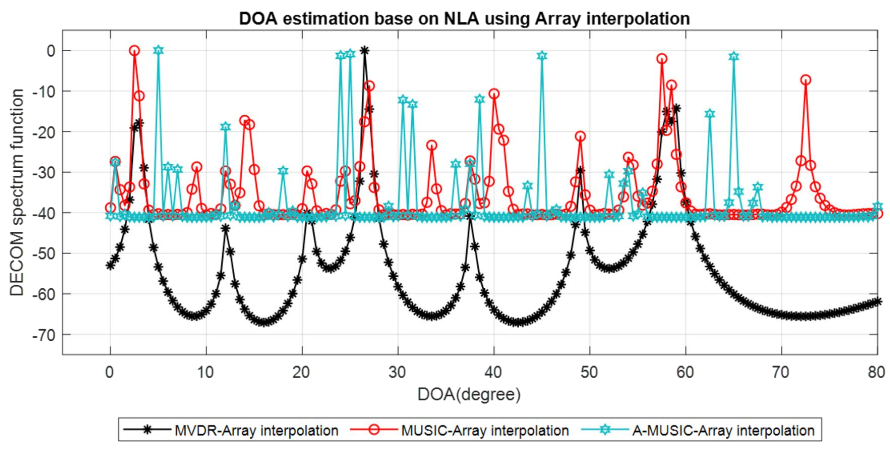
DOA estimation base on NLA using Array interpolation
DECOM spectrum function
0
-10
-20
-30
-40
-50
-60
-70
0
10
20
30
40
50
60
70
80
DOA(degree)
MVDR-Array interpolation
MUSIC-Array interpolation
A-MUSIC-Array interpolation

Figure 7(c).

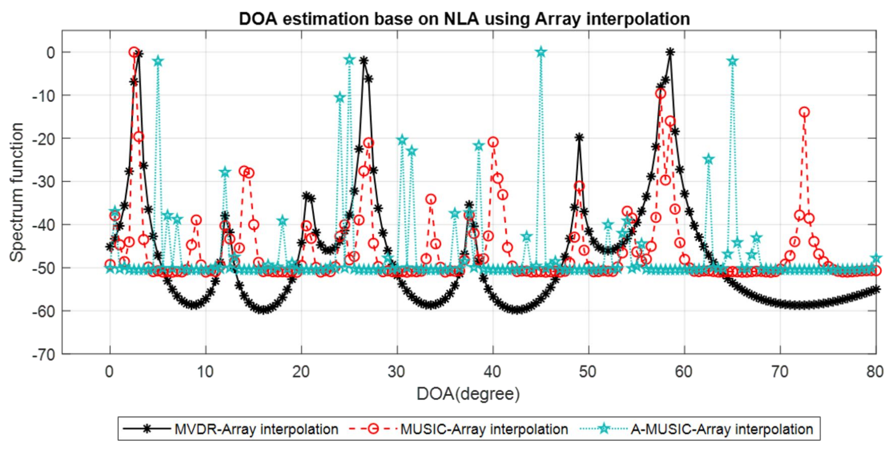

DOA estimation base on NLA using Array interpolation
Spectrum function
0
-10
-20
-30
-40
-50
-60
-70
0
10
20
30
40
50
60
70
80
DOA(degree)
MVDR-Array interpolation
MUSIC-Array interpolation
A-MUSIC-Array interpolation

Figure 7(d).

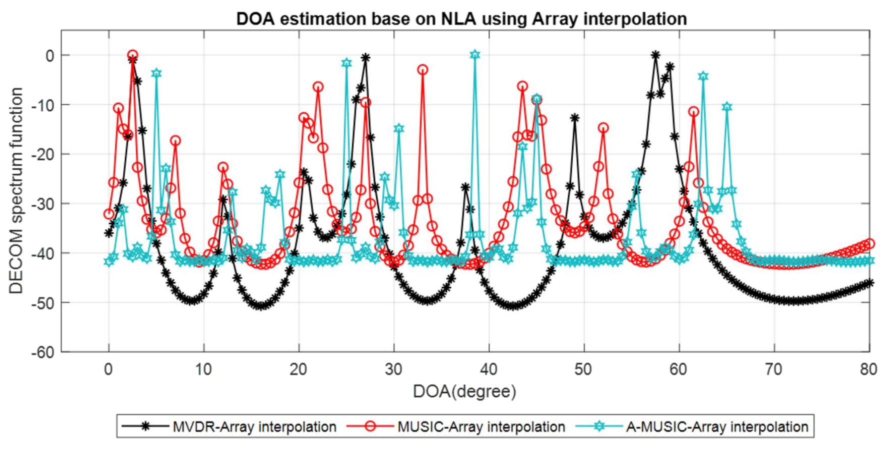
DOA estimation base on NLA using Array interpolation
DECOM spectrum function
DOA(degree)
0
-10
-20
-30
-40
-50
-60
0
10
20
30
40
50
60
70
80
MVDR-Array interpolation
MUSIC-Array interpolation
A-MUSIC-Array interpolation

Figure 8(a).

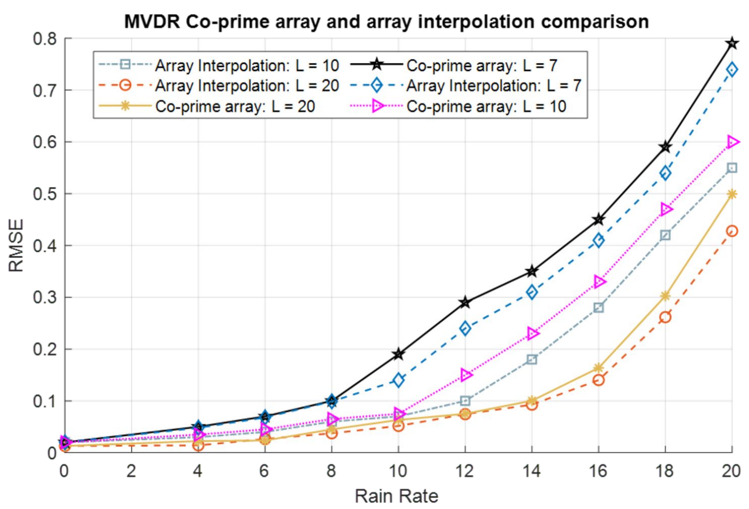

MVDR Co-prime array and array interpolation comparison
Array Interpolation: L = 10
Array Interpolation: L = 20
Co-prime array: L = 20
Co-prime array: L = 7
Array Interpolation: L = 7
Co-prime array: L = 10
RMSE
Rain Rate
0
0.1
0.2
0.3
0.4
0.5
0.6
0.7
0.8
0
2
4
6
8
10
12
14
16
18
20

Figure 8(b).

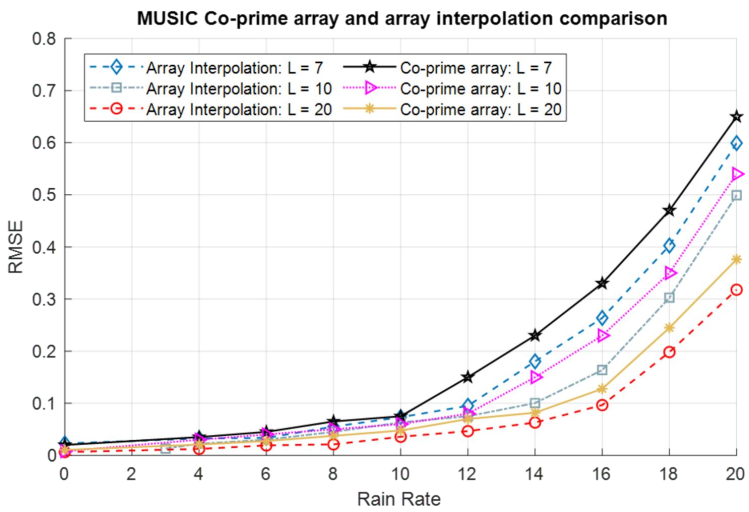

MUSIC Co-prime array and array interpolation comparison
Array Interpolation: L = 7
Array Interpolation: L = 10
Array Interpolation: L = 20
Co-prime array: L = 7
Co-prime array: L = 10
Co-prime array: L = 20
RMSE
Rain Rate
0
0.1
0.2
0.3
0.4
0.5
0.6
0.7
0.8
2
4
6
8
10
12
14
16
18
20

Figure 8(c).

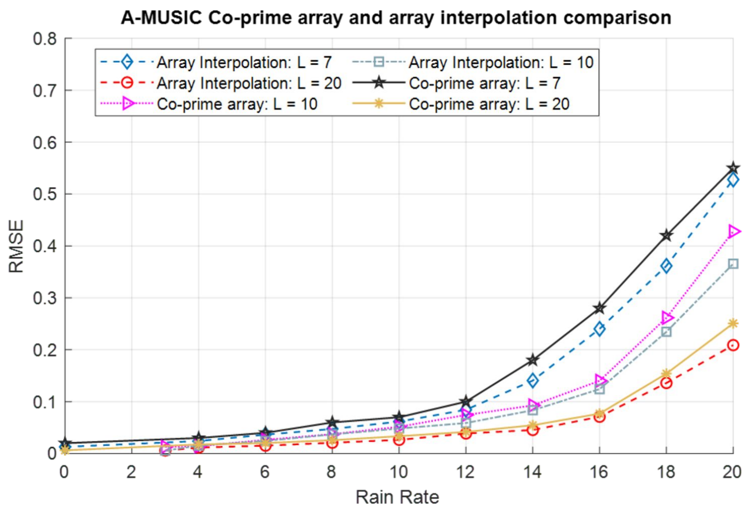

A-MUSIC Co-prime array and array interpolation comparison
Array Interpolation: L = 7
Array Interpolation: L = 10
Array Interpolation: L = 20
Co-prime array: L = 7
Co-prime array: L = 10
Co-prime array: L = 20
RMSE
0
0.1
0.2
0.3
0.4
0.5
0.6
0.7
0.8
Rain Rate
0
2
4
6
8
10
12
14
16
18
20

Figure 9(a).

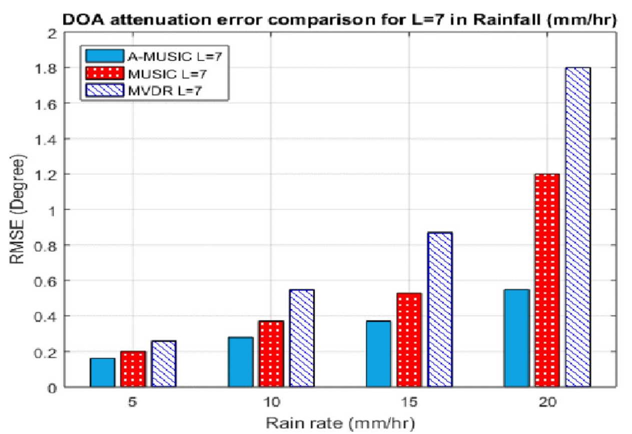

DOA attenuation error comparison for L=7 in Rainfall (mm/hr)
A-MUSIC L=7
MUSIC L=7
MVDR L=7
RMSE (Degree)
Rain rate (mm/hr)
0
0.2
0.4
0.6
0.8
1
1.2
1.4
1.6
1.8
2
5
10
15
20

Figure 9(b).

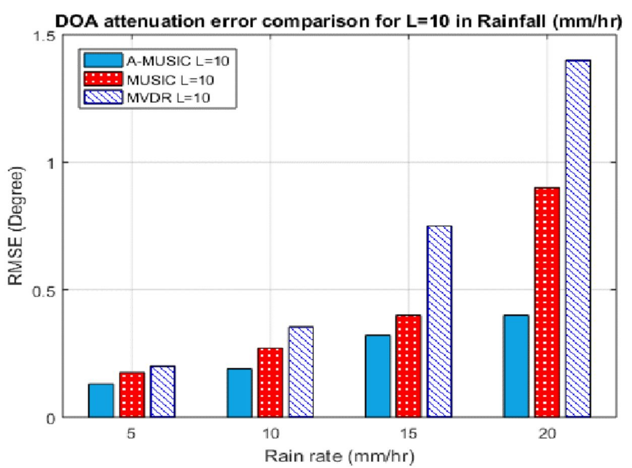
DOA attenuation error comparison for L=10 in Rainfall (mm/hr)
A-MUSIC L=10
MUSIC L=10
MVDR L=10
RMSE (Degree)
0
0.5
1
1.5
5
10
15
20
Rain rate (mm/hr)

Figure 9(c).

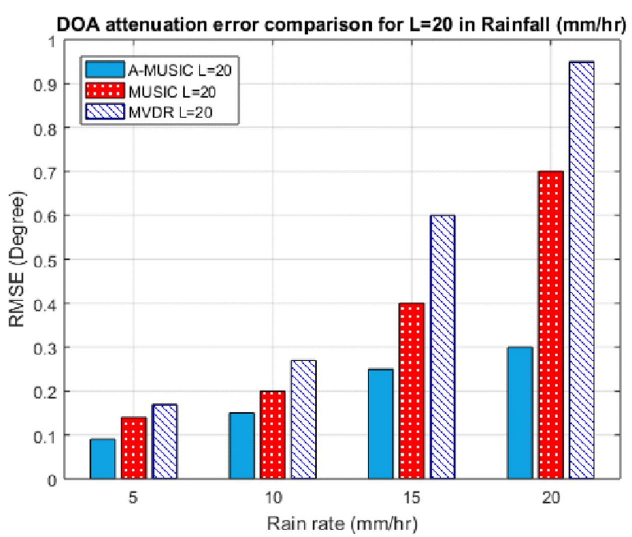
DOA attenuation error comparison for L=20 in Rainfall (mm/hr)
A-MUSIC L=20
MUSIC L=20
MVDR L=20
RMSE (Degree)
Rain rate (mm/hr)
0
0.1
0.2
0.3
0.4
0.5
0.6
0.7
0.8
0.9
1
5
10
15
20

Figure 10.

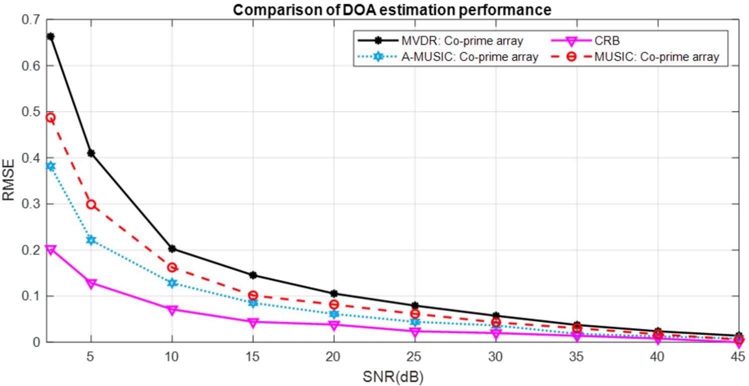
Comparison of DOA estimation performance
MVDR: Co-prime array
A-MUSIC: Co-prime array
CRB
MUSIC: Co-prime array
RMSE
SNR(dB)
0
0.1
0.2
0.3
0.4
0.5
0.6
0.7
5
10
15
20
25
30
35
40
45

Figure 11.

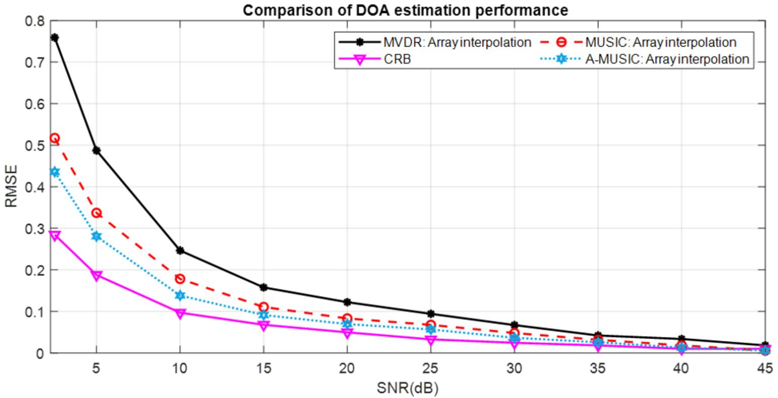
Comparison of DOA estimation performance
MVDR: Array interpolation
MUSIC: Array interpolation
CRB
A-MUSIC: Array interpolation
RMSE
SNR(dB)
0.8
0.7
0.6
0.5
0.4
0.3
0.2
0.1
0
5
10
15
20
25
30
35
40
45

Figure 12.

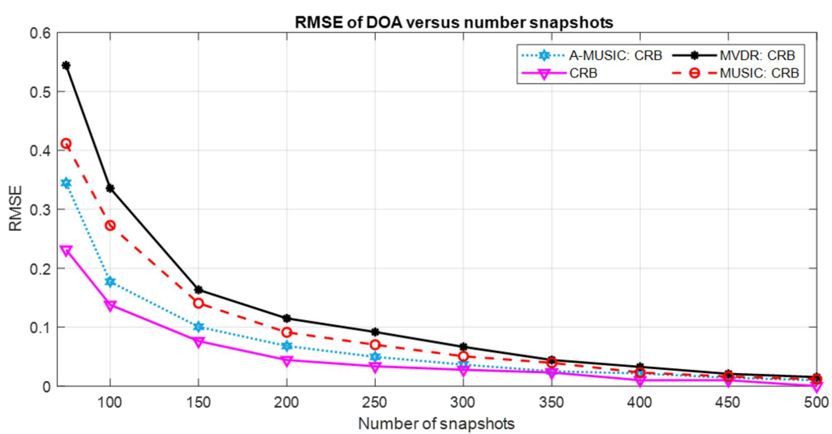
RMSE of DOA versus number snapshots
RMSE
Number of snapshots
0
0.1
0.2
0.3
0.4
0.5
0.6
100
150
200
250
300
350
400
450
500
A-MUSIC: CRB
MVDR: CRB
CRB
MUSIC: CRB

Figure 13.

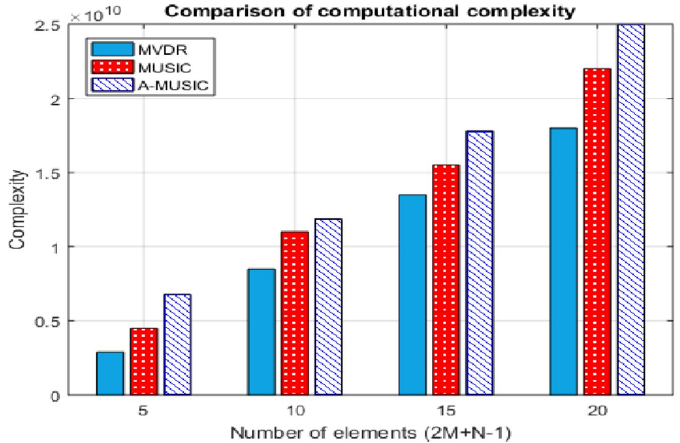

Comparison of computational complexity
×10^10
2.5
2
1.5
1
0.5
0
Complexity
MVDR
MUSIC
A-MUSIC
5
10
15
20
Number of elements (2M+N-1)